A state estimate of Siberian summer temperature and moisture availability during the Last Glacial Maximum combining pollen records and climate simulations

Nils Weitzel[1,2], Andreas Hense[3], Ulrike Herzschuh[4,5,6], Thomas Böhmer[4], Xianyong Cao[7], Kira Rehfeld[1,2]

[1] Institute of Environmental Physics, Heidelberg University, Heidelberg, Germany

[2] Geo- und Umweltforschungszentrum, Dept. of Geosciences, Eberhard Karls Universität Tübingen, Tübingen, Germany

[3] Institute of Geosciences, Sect. Meteorology, University of Bonn, Bonn, Germany

[4] Alfred-Wegener-Institut Helmholtz-Zentrum für Polar- und Meeresforschung, Research Unit Potsdam, Potsdam, Germany

[5] Institute of Environmental Sciences and Geography, University of Potsdam, Potsdam, Germany

[6] Institute of Biochemistry and Biology, University of Potsdam, Potsdam, Germany

[7] Alpine Paleoecology and Human Adaptation Group,
State Key Laboratory of Tibetan Plateau Earth System, and Resources and Environment,
Institute of Tibetan Plateau Research, Chinese Academy of Sciences, Beijing, China

Correspondence: Nils Weitzel (nweitzel@iup.uni-heidelberg.de)

The Last Glacial Maximum (LGM, ∼21.000 years before present) was a period with significantly lower global mean temperature, large Northern Hemisphere ice sheets, and low CO_2 concentrations. Unlike other high-latitude areas, Siberia was not covered by a terrestrial ice sheet. Climate simulations with LGM boundary conditions show large inter-model differences especially in Northern Siberia, which impede a direct analysis of Siberian LGM climate from simulations. Thus, constraints from proxy data are needed. Here, we reconstruct summer temperature and moisture availability from a network of Siberian pollen records using statistical transfer functions. The estimates are corrected for the lower CO_2 concentrations during the LGM with an a posteriori method. Using a Bayesian framework, we combine the pollen-based reconstructions with climate simulations to obtain the first regional state estimate of LGM climate constrained by proxies from Central and Eastern Siberia. Our reconstruction shows higher summer temperature anomalies than most high-latitude areas and simulations. Reconstructed moisture availability is similar to present-day values, consistent with most simulations. Analyses of the simulations show that anomalous circulation patterns and reduced cloud cover contribute particularly to the relatively high summer temperatures, supporting previous studies based solely on climate simulations. Our data-constrained state estimate is well-suited for future analyses of Siberian LGM climate such as investigations of the reasons for the absence of a Siberian ice sheet during the LGM.

1 Introduction

During the Last Glacial Maximum (LGM), $\sim 21,000$ years before present (21ka), the global mean temperature was significantly lower than today. Large parts of North America, Greenland, and Fennoscandia were covered by ice sheets (Batchelor et al., 2019), the CO_2 concentration was less than half of present-day values with around 185 ppm (Köhler et al., 2017), and sea level was around 120 m lower than currently (Lambeck et al., 2014). Seasonal insolation differences were reduced in both hemispheres (Otto-Bliesner et al., 2006). These deviations from present-day conditions make the LGM an important period for studying the Earth system and evaluating climate models (Kageyama et al., 2017).

We focus on the Siberian LGM climate east of the Jenissei river (Fig. 1). Our study domain is structured by the major rivers Jenissei, Lena and Kolyma. It extends to the Arctic Ocean in the north, the Pacific Ocean in the East, and south to Lake Baikal and the Amur river. Major topographic features are medium elevation highlands between Jenissei and Lena (Central Siberia) and highlands east of the Lena (Eastern Siberia / Western Beringia). Today, most of Siberia is exposed to a very continental climate with decreasing precipitation from Western (500 – 800 mm per year) to Eastern Siberia (100 – 400 mm per year). Only in a small sector along the Pacific Ocean, precipitation rates are higher. Low temperatures and dry conditions in winter facilitate the forming of a persistent Siberian high pressure system, whereas a Siberian low is the dominant pressure system in summer. Mean July temperatures are as high as 20°C in southern Siberia but only around 10°C in the northernmost parts.

As the Siberian shelf is mostly shallow, the lower sea level during the LGM led to a closed Bering strait and a northward retreat of the Arctic Ocean by several hundreds of kilometers (Fig. 1). However, unlike other high-latitude areas on the Northern Hemisphere, Siberia was not covered by a large terrestrial ice sheet. Only the most northwestern part of our reconstruction domain was covered by the Barents-Kara ice sheet (Fig. 1, Hughes et al., 2015; Abe-Ouchi et al., 2015). The maximum Siberian glacier extent was probably reached around 90ka (Hughes et al., 2013), followed by a subsequent glacier retreat in connection with increased Fennoscandian glaciation, which was only interrupted by a minor glacial advance around 50ka (Svendsen et al., 2004; Stauch and Gualtieri, 2008). In the Pacific sector glaciers were near present-day extension during the LGM (Stauch and Gualtieri, 2008; Meyer and Barr, 2017).

Information on Siberian climatic conditions during the LGM are available from pollen records (e.g. Tarasov et al., 1999), macrofossils (e.g. Kienast et al., 2005), faunal remains (e.g. Sher et al., 2005), boreholes (e.g. Dorofeeva et al., 2002), stable isotopes in ice wedges (e.g. Meyer et al., 2002), and diatoms and biogenic silica (e.g. Colman et al., 1995). Borehole temperature reconstructions of the last glacial cycle at Lake Baikal show minimal mean annual temperatures around 90ka and a subsequent temperature increase leading to an LGM anomaly of ~ -4 K compared to present-day (Dorofeeva et al., 2002). Dryer conditions than today are consistently reconstructed from a variety of proxies (e.g. Tarasov et al., 1999; Wu et al., 2007a; Andreev et al., 2011; Opel et al., 2019). Only in the Pacific sector, precipitation amounts might have been similar to today (Meyer and Barr, 2017). Strongly reduced winter temperatures are reconstructed from pollen records (e.g. Tarasov et al., 1999; Wu et al., 2007a), stable isotopes (e.g. Wetterich et al., 2021), and macrofossils (e.g. Andreev et al., 2011). In contrast, inconsistent results are reported from various proxies for summer temperature (e.g. Tarasov et al., 1999; Kienast et al., 2005; Wu et al., 2007a; Lozhkin et al., 2007; Andreev et al., 2011; Berman et al., 2011). Joint reconstructions of summer and winter temperature for Western Siberia indicate increased seasonal temperature differences (Tarasov et al., 1999; Wu et al., 2007a). Despite these efforts, Siberia is currently underrepresented in terrestrial compilations of LGM climate reconstructions. While records from Western Siberia and the Lake Baikal region are included in regional (Tarasov et al., 1999; Wu et al., 2007a) and global compilations (Bartlein et al., 2011; Cleator et al., 2020), records from Central and Eastern Siberia are absent from these datasets.

As a core period of the Paleoclimate Modelling Intercomparison Project (PMIP), LGM simulations have been run with a wide range of climate models. Bakker et al. (2020) note a large PMIP3 inter-model spread for Siberian summer temperature anomalies with ensemble spreads of more than 20 K in some regions. Niu et al. (2019) show that a numerical ice sheet model grows a Siberian ice sheet for summer temperatures below ~ -5°C. This threshold is crossed in Northern Siberia in three PMIP3 simulations. Bakker et al. (2020) find that simulated summer temperatures in Siberia react very sensitively to the

employed ice sheet topography and model specification, in particular physics parameterizations. This sensitivity makes the analysis of Siberian LGM climate from climate simulations very dependent on the selected model such that conclusions derived purely from simulations could deviate strongly from reality. Therefore, joint analyses of simulations and proxy data are needed.

To get a better constrained state estimate of LGM climate conditions, we compile published pollen records from Central and Eastern Siberia (Cao et al., 2020; Herzschuh et al., 2022c) with harmonized taxonomy and age models (Li et al., 2021; Herzschuh et al., 2022c,a) (see Sect. 2.1). For the 33 records in the compilation with samples during the LGM, we reconstruct July temperature (T_{Jul}) and moisture availability, quantified by the moisture index (MI) of mean annual precipitation over potential evapotranspiration, using weighted averaging partial least squares (WAPLS, Birks et al., 2010) (see Sect. 3.1). This statistical transfer function exploits pollen-climate relationships in a modern calibration dataset. Reconstructions of glacial climates with WAPLS can be biased due to the ecophysiological effects of the lower CO_2 concentration which are not incorporated in the transfer functions (Chevalier et al., 2020, and the references therein). To circumvent this problem, previous studies inverted numerical vegetation models in which the ecophysiological effects of changing CO_2 conditions are simulated (e.g. Guiot et al., 2000; Wu et al., 2007a; Izumi and Bartlein, 2016). However, these reconstructions depend strongly on the CO_2-sensitivity in the employed model, which differs widely across models (e.g. Cramer et al., 2001; Adam et al., 2021), and the uncertain mapping of vegetation classes in models (plant functions types) to taxa identified in pollen samples. An alternative using an eco-optimality-based theoretical model for carbon uptake (Prentice et al., 2014; Wang et al., 2017) was developed recently (Prentice et al., 2017; Cleator et al., 2020; Wei et al., 2021). In this approach, reconstructions from statistical transfer functions are corrected a posteriori to account for the lower CO_2 concentrations. Theory (Williams et al., 2000; Prentice et al., 2017) and recent inverse modelling studies (Izumi and Bartlein, 2016; Wu et al., 2019) suggest that moisture availability reconstructions are biased dry when not accounting for lower CO_2 concentrations, whereas the influence on temperature reconstructions is small. Therefore, we correct the WAPLS-based MI reconstructions with the algorithm from Wei et al. (2021), whereas we do not alter the WAPLS-based T_{Jul} reconstructions (see Sect. 3.1).

The spatial distribution of our pollen sample network is too coarse to create gridded maps with simple statistical interpolation. Therefore, we use Bayesian statistics to combine the local reconstructions with a multi-model ensemble of climate simulations from the PMIP3 and PMIP4 projects (Braconnot et al., 2011, 2012; Kageyama et al., 2021) to compute a state estimate of Siberian LGM climate (see Sect. 2.3, 3.2). In the state estimate, the proxy data provides local climate information whereas the spatial interpolation between proxy records is controlled by the simulations and a residual stochastic field (Weitzel et al., 2019). The result is a spatially distributed probability distribution. Existing regional compilations (Tarasov et al., 1999) and global state estimates (Annan and Hargreaves, 2013; Cleator et al., 2020; Tierney et al., 2020) do not contain local reconstructions from Central and Eastern Siberia. Thus, we provide the first gridded reconstruction of Central and Eastern Siberian LGM climate constrained by pollen records from this region (see Sect. 4.2). None of the previous state estimates uses simulations from the PMIP4 ensemble. We are not just relying on a single model (Tierney et al., 2020) or the ensemble mean and standard deviation (Cleator et al., 2020) as these strategies are prone to biases considering the high model-dependency of simulated Siberian LGM climate (Bakker et al., 2020). Unlike previous state estimates, we include additional non-Gaussian elements and a proxy-constrained residual stochastic field to better account for non-Gaussian ensemble member statistics and structural model-data differences.

We use the estimated ensemble member weights to understand differences in the simulations that control the fit with the data (Sect. 4.2). We show that the ensemble member fit depend on summer temperature deviations from the ensemble mean in Northern Eurasia. These deviations are related to anomalous atmospheric circulation and cloud cover patterns, which supports findings from modelling studies (Löfverström et al., 2014; Bakker et al., 2020).

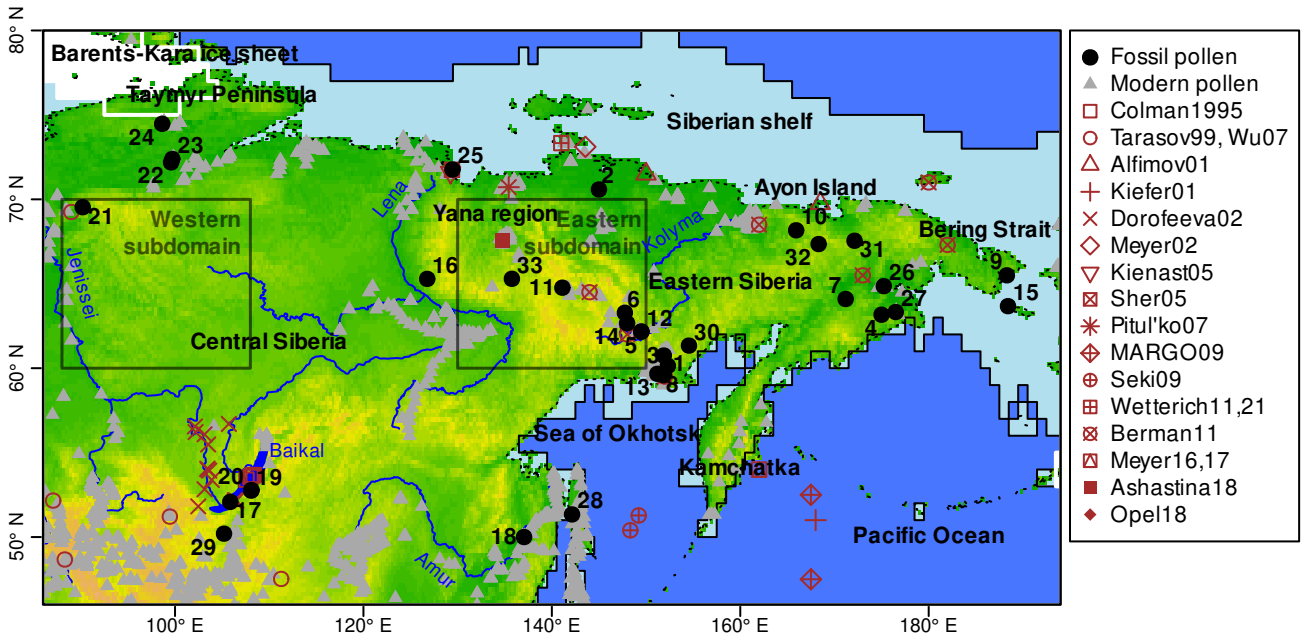

Figure 1: Spatial domain of this study. Pollen records included in the state estimate are marked by black dots. Modern pollen samples are depicted by gray triangles. Records mentioned in the manuscript from previous studies are shown in brown symbols (see Table 3 for the full references of the studies). The LGM coastline (Abe-Ouchi et al., 2015) is denoted by thick black lines, the modern coastline by dotted lines, the Siberian shelf by shaded blue surfaces, and the PMIP3 LGM ice sheet extent in the northwestern part of the domain (Abe-Ouchi et al., 2015) by white surfaces and white lines. The two rectangles denote the eastern and western subdomains that are further studied in Sect. 4.2 and Fig. 7. The background topography is from Amante and Eakins (2009).

Table 1: Information on the locations, modern climate, calibration data climatic ranges, number of WAPLS components, number of modern samples included in the transfer function, and references of the fossil pollen records.

ID	Name	Lon [°]	Lat [°]	Modern T_{Jul} [°C]	Range T_{Jul} [°C]	Modern MI [m/m]	Range MI [m/m]	Comp. T_{Jul}	Comp. MI	Number of samples	References
1	Alut Lake	152.3	60.1	12	[0.9, 22.5]	1.1	[0.39, 2.37]	2	1	962	Anderson et al. (1998b)
2	Berelyekh River	145	70.6	10.5	[-2.5, 18.7]	0.6	[0.39, 2.21]	1	1	866	Lozhkin and Postolenko (1989)
3	Elikchan 4 Lake	151.9	60.8	12.5	[0.9, 21.5]	0.98	[0.39, 2.37]	2	2	931	Lozhkin A. V. and Anderson (1995) Lozhkin et al. (1995)
4	Gytgykai Lake	175	63.2	9.5	[0.9, 16.5]	1.34	[0.25, 2.36]	1	2	851	Lozhkin et al. (1998a)
5	Jack London Lake	149.5	62.2	12.9	[0.9, 21.5]	0.89	[0.39, 2.36]	2	2	920	Lozhkin et al. (1993)
6	Berelyekh River	147.8	63.3	13	[0.9, 21.5]	0.8	[0.39, 2.36]	2	2	928	Lozhkin (1998)
7	Ledovyi Obryu	171.2	64.1	13.9	[0.9, 18.3]	1.12	[0.25, 2.36]	1	2	886	Lozhkin et al. (2000)
8	Lesnoye Lake	151.9	59.6	10.9	[0.9, 22.5]	1.27	[0.39, 2.37]	2	2	978	Anderson et al. (1997) Anderson and Lozhkin (2002)
9	Lorino Exposure	-171.7	65.5	8.4	[0.9, 16.9]	1.95	[0.25, 4]	1	1	889	Ivanov (1986) Anderson and Lozhkin (2002)
10	Enmynveem River	165.9	68.2	11.6	[0.9, 18.7]	0.61	[0.25, 2.36]	1	2	1063	Lozhkin et al. (1988)
11	Smorodinovoye Lake	141.1	64.8	13.7	[0.9, 21.5]	0.79	[0.39, 2.36]	2	2	1060	Anderson et al. (1998a)
12	Sosednee	149.5	62.2	12.9	[0.9, 21.5]	0.89	[0.39, 2.36]	2	2	920	Lozhkin et al. (1993)
13	Tanon River	151.2	59.7	13	[0.9, 22.5]	1.26	[0.39, 2.37]	2	2	988	Lozhkin and Glushkova (1997)
14	Kirgirlakh Stream_2	148	62.7	14	[0.9, 21.5]	0.83	[0.39, 2.36]	2	2	921	Shilo et al. (1983)
15	St. Lawrence Island Sec. 3	-171.6	63.7	8	[0.9, 16.5]	1.98	[0.25, 4]	1	1	840	Lozhkin et al. (1998b)
16	Lake Billyakh_PG1755	126.8	65.3	15.7	[-2.5, 21.6]	0.72	[0.35, 2.2]	1	1	1159	Müller et al. (2010)
17	Lake Baikal	105.9	52.1	13.8	[-2, 33]	0.81	[0.02, 1.68]	1	1	2360	Demske et al. (2005)
18	Gur	137.1	50	20.3	[7.8, 27.1]	1.24	[0.17, 3.96]	1	2	1701	Mokhova et al. (2009)
19	Cheremushka Bog	108.1	52.8	16.6	[-2, 33]	0.61	[0.02, 1.68]	1	1	2263	Shichi et al. (2009)
20	Lake Kotokel_2010	108.1	52.8	16.9	[-2, 33]	0.61	[0.02, 1.68]	1	1	2262	Tarasov et al. (2009) Bezrukova et al. (2010)
21	Lake Lama	90.2	69.5	11.7	[-2.5, 21.6]	1.45	[0.36, 1.87]	2	2	1328	Andreev et al. (2004)
22	LAO13-94	99.6	72.2	9.6	[-2.5, 19]	0.96	[0.39, 1.87]	2	2	978	Andreev et al. (2002)
23	LAO6-96	99.7	72.4	10	[-2.5, 19]	0.96	[0.39, 1.87]	2	2	982	Andreev et al. (2002)
24	Levinson-Lessing Lake	98.6	74.5	6.6	[-2.5, 18.7]	0.94	[0.39, 1.87]	2	2	924	Andreev et al. (2003)
25	Mamontovy Khayata	129.5	71.8	6.4	[-2.5, 18.7]	0.65	[0.39, 1.87]	1	1	898	Andreev et al. (2000)
26	Melkoye Lake	175.2	64.9	12.4	[0.9, 16.5]	1.18	[0.25, 2.47]	1	2	877	Lozhkin and Anderson (2013)
27	Patricia Lake	176.5	63.3	9.6	[0.9, 16.5]	1.47	[0.25, 2.47]	1	2	860	Anderson and Lozhkin (2015)
28	Sakhalin Island_Khoe	142.1	51.3	13.2	[8.2, 26.7]	1.33	[0.28, 3.09]	2	2	1377	Leipe et al. (2015)
29	Shaamar	105.2	50.2	17.4	[-2, 33]	0.8	[0.02, 1.68]	1	1	2519	Ma et al. (2013)
30	Julietta Lake	154.6	61.3	12.4	[0.9, 21.4]	1.04	[0.39, 2.37]	2	2	862	Anderson et al. (2010)
31	Elgygytgyn Lake	172.1	67.5	3.3	[0.9, 18.3]	0.82	[0.25, 2.36]	1	2	965	Melles et al. (2012) Lozhkin et al. (2007)
32	Ilierney	168.3	67.4	6.6	[0.9, 18.7]	0.83	[0.25, 2.36]	1	2	1037	Vyse et al. (2020)
33	Emanda	135.8	65.3	12.6	[-2.5, 21.5]	0.68	[0.39, 2.36]	2	2	1100	Baumer et al. (2021)

2 Data

2.1 Fossil pollen samples

To compute local T_{Jul} and MI reconstructions, we use a compilation of pollen records, which are located between 90°E and 171°W and 50°N and 75°N. The records are part of a new global pollen dataset with harmonized age models (Li et al., 2021; Herzschuh et al., 2022c). For each record, the raw radiocarbon dates as well as pollen percentages or counts had to be available to be included in the synthesis. Harmonized age models were computed with the Bayesian age model Bacon (Blaauw and Christen, 2011) and the IntCal20 calibration curve (Reimer et al., 2020) as described in Li et al. (2021). We select all samples in the reconstruction domain from the global compilation with calibrated mean ages between 19ka and 23ka. This interval is the same as in previous global compilations (e.g. Bartlein et al., 2011). These criteria led to 209 samples from 33 records (see Table 1, Fig. 1).

The taxonomy of the pollen records were harmonized (Herzschuh et al., 2022a,c). Major tree and shrub pollen as well as very common herbaceous taxa (e.g. Artemisia, Thalictrum, Rumex) were merged to genus level and remaining herbaceous taxa to family level. Aquatic pollen except for Cyperaceae, spores from ferns and fungi, and algae were excluded. Pollen percentages for all samples were computed from the respective pollen counts. For the reconstructions, the 70 most common taxa in Asia based on Hill's N2 diversity index (Hill, 1973) were selected. This number provides a compromise between using the information from the occurring biodiversity and having sufficient coverage in the modern training data to identify the bioclimatic niches of the individual taxa. For more details, see Herzschuh et al. (2022a).

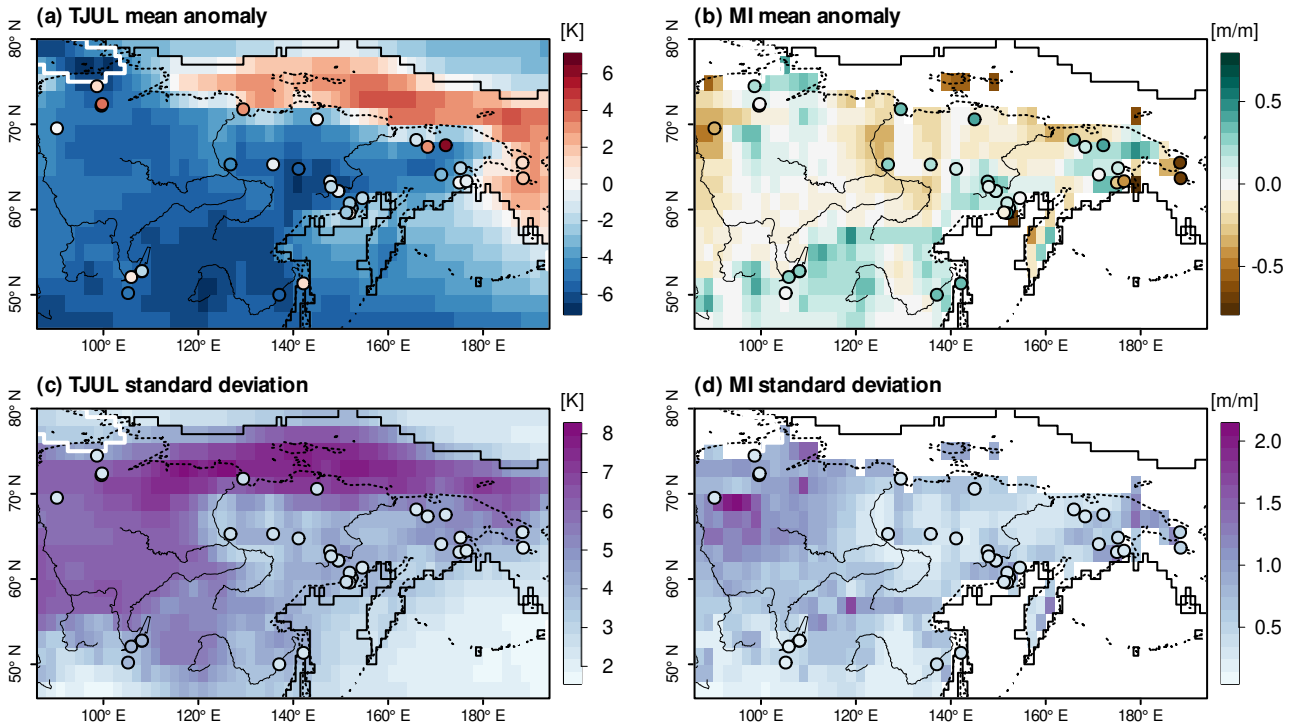

Figure 2: Simulation ensemble statistics (in the background) and local reconstructions (colored dots), (a) T_{Jul} mean anomalies, (b) MI mean anomalies, (c) T_{Jul} standard deviation, (d) MI standard deviation. The LGM coastline is denoted by thick black lines, the modern coastline by dotted lines, major rivers by thin black lines, and the PMIP3 LGM ice sheet extent by a white line.

2.2 Modern pollen and climate data

To calibrate statistical pollen-climate transfer functions, we use modern pollen and climate datasets. The modern pollen samples are selected from a Northern Hemisphere calibration dataset comprised of 15,379 samples, which includes previous compilations for Eurasia and North America (Herzschuh et al., 2022a). The taxonomy of these samples is harmonized following the same strategy as for the fossil pollen data. For each fossil pollen record, an individual transfer function model is fitted using only the modern samples in a 2000 km radius around the record location. The locations of the modern samples in the reconstruction domain are shown in Fig. 1 and the radius for each record is given in Online Resource 1. For more information on the modern dataset see Herzschuh et al. (2022a).

We derive modern climatologies from the WorldClim 2 dataset (Fick and Hijmans, 2017) with a spatial resolution of 1 km. From this dataset, we extract T_{Jul}, mean annual temperature (T_{ann}) and annual precipitation (P_{ann}). Additionally, we use the annual potential evapotranspiration (PET_{ann}) dataset from CRU TSv4.03 (Harris et al., 2020), as WorldClim does not contain PET in its set of bioclimatic variabiables. Following (Prentice et al., 2017), we compute MI as

$$\mathrm{MI} = \frac{P_{ann}}{PET_{ann}}. \quad (1)$$

The PET dataset has a lower resolution than the WorldClim data. Therefore, we interpolate it to the grid of the P_{ann} dataset. For each pollen site, we interpolate the gridded climate datasets to the locations of the sites. Compared to other reconstruction uncertainties, we consider the errors from these interpolation steps to be negligible.

2.3 Climate simulation output

We employ a multi-model ensemble of climate simulations from the PMIP3 and PMIP4 projects (Braconnot et al., 2011, 2012; Kageyama et al., 2021). These serve as a second input besides the pollen-based

Table 2: Information on the PMIP3 and PMIP4 climate simulation ensemble.

Model	Institute	GMST anomaly [K]	Siberian T_{Tjul} anomaly [K]	Siberian MI anomaly [m/m]	PMIP generation	Reference
CCSM4	NCAR	-4.9	-5.8	-0.14	PMIP3	Gent et al. (2011)
COSMOS-ASO	FUB	-5.5	-3.0	-0.23	PMIP3	Budich et al. (2010)
FGOALS-g2	LASG-CESS	-4.6	-5.7	-0.17	PMIP3	Li et al. (2013)
GISS-E2-R	NASA-GISS	-4.8	-12.6	+0.93	PMIP3	Schmidt et al. (2014)
IPSL-CM5A-LR	IPSL	-4.6	-2.8	-0.23	PMIP3	Dufresne et al. (2013)
MIROC-ESM	MIROC	-5.0	-6.7	-0.16	PMIP3	Sueyoshi et al. (2013)
MPI-ESM-P	MPI-M	-4.4	-1.8	-0.42	PMIP3	Giorgetta et al. (2013)
MRI-CGCM3	MRI	-4.7	-1.1	-0.53	PMIP3	Yukimoto et al. (2012)
AWI-ESM-1-1-LR	AWI	-3.7	-1.7	-0.30	PMIP4	Sidorenko et al. (2015)
INM-CM4-8	INM	-3.7	-1.5	-0.19	PMIP4	Volodin et al. (2018)
MIROC-ES2L	MIROC	-4.0	-2.2	-0.43	PMIP4	Hajima et al. (2020)
MPI-ESM1-2-LR	MPI-M	-3.9	-1.1	-0.44	PMIP4	Mauritsen et al. (2019)

reconstructions to infer the gridded state estimates of T_{Jul} and MI. The boundary conditions in the simulations were adjusted to the LGM, including changed orbital configurations, greenhouse gas concentrations, ice sheets, and topography (Braconnot et al., 2011; Abe-Ouchi et al., 2015; Kageyama et al., 2017). Note that the boundary conditions of PMIP3 and PMIP4 are not equal, such that the ensemble spread is a result from inter-model variability and boundary condition changes from PMIP3 to PMIP4. As ideally the ensemble spread would represent the physically reasonable climate states during the LGM, this additional source of variability does not hamper our state estimates. The PMIP3 runs are based on CCSM4, COSMOS-ASO, FGOALS-g2, GISS-E2-R, IPSL-CM5A-LR, MIROC-ESM, MPI-ESM-P, and MRI-CGCM3 models and the PMIP4 runs include simulations from AWI-ESM-1-1-LR, INM-CM4-8, MIROC-ES2L, and MPI-ESM1-2-LR (Table 2). The models were run until an equilibrium state was obtained (spin-up), after which simulations were continued and archived for at least 100 years.

We interpolate all simulations to a common 2° by 2° grid. The climatological means for the respective reconstruction variables are extracted. This minimizes inter-annual to decadal variability, which is not resolved by the pollen-based reconstructions. We compute anomalies with respect to pre-industrial (PI) simulations with the same models. PET is not directly available from data repository. We compute it by applying the formula developed by Hargreaves (1994). Compared to the often-used Penman-Monteith formula it has the advantage of needing less input data and it performed comparable to the Penman-Monteith formula but was less sensitive to climate biases in a large-scale test by Trabucco et al. (2008). As PET formulas are developed and tested only over ice-free land, we exclude areas which were ocean or land ice during either the LGM or PI from the MI reconstruction.

Based on the pollen record compilation, our spatial domain for the state estimate is a regular lat-lon grid which extends from 87°E to 167°W and from 47°N to 79°N. Fig. 2 shows the simulation ensemble means and standard deviations of T_{Jul} and MI. The T_{Jul} ensemble mean anomaly in the reconstruction domain is -3.8 K with a standard deviation of 3.4 K. Anomalies are largest in continental Siberia and smallest along the Arctic Ocean coastline. The change from sea to land on the Siberian shelf leads to positive T_{Jul} anomalies in the area above sea level during the LGM. The ensemble spread is largest along the Arctic Ocean coastline and in Central Siberia. For MI, the ensemble mean anomaly across the domain is +0.01 m/m and thus virtually equal to present-day. The ensemble standard deviation is 0.51 m/m. The moisture availability tends to be reduced in Northern Siberia and increased along the Pacific Ocean coastline. The largest ensemble standard deviations occur in Central Siberia.

3 Methods

In this section, we describe the inference strategy for the local reconstructions and the methodology of the state estimates combining pollen-based reconstructions and simulation ensemble (Fig. 3).

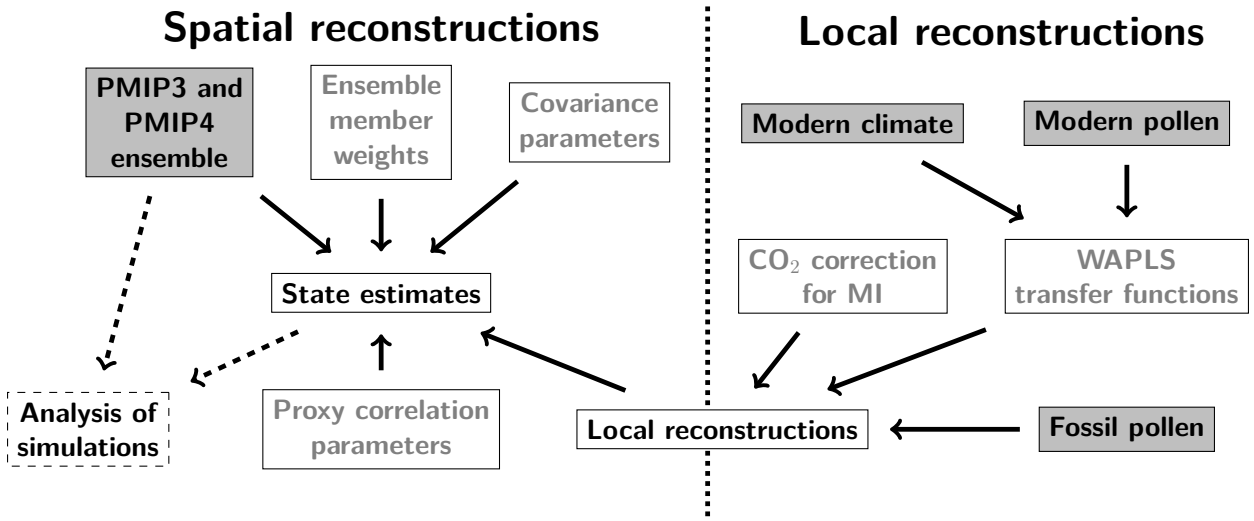

Figure 3: Graph of the workflow for local reconstructions (right hand side) and state estimates (left hand side). Involved quantities are given by nodes. Nodes with gray background denote input data and nodes with gray font are statistical model parameters. Arrows indicate contributions to the output products.

3.1 Local reconstructions

3.1.1 Statistical transfer functions

Local reconstructions from each pollen sequence are inferred with WAPLS transfer functions (Ter Braak and Juggins, 1993; Ter Braak et al., 1993) following the methodology from Herzschuh et al. (2022a). WAPLS is a regression-based statistical transfer function that consists of two stages (Birks et al., 2010). First, the climate optimum of each taxa is estimated based on the modern calibration dataset. Second, the climate optima are weighted according to the pollen percentages in the fossil pollen sample to obtain a local climate reconstruction. Partial least squares regression is used to account for residual correlations in the training data not explained by the respective climate variable. Uncertainty estimates are calculated using the bootstrapped RMSEP from cross-validation of the modern calibration dataset (Juggins, 2020). Due to the absence of core top samples for several records, LGM anomalies are calculated with respect to the calibration climatology. The pollen percentages are square-root transformed prior to computing the transfer functions. The number of used WAPLS components is selected from a randomization t-test (Juggins and Birks, 2012; van der Voet, 1994). Depending on the test results either one or two components for each of the records are chosen (see Table 1).

For each proxy record, modern samples within a 2000 km radius are used for calibration. This distance provides a sufficient ecological and climatic range to estimate pollen-climate relationships and resolve glacial-interglacial vegetation differences (see Table 1). However, it limits the occurrence of spurious analogues (Cao et al., 2014) and of multi-modal taxa responses, which can result from the limited taxonomic resolution of the datasets because multiple species can be aggregated to the same genus. The avoidance of multi-modal taxa responses is important because the WAPLS regression relies on the assumption of a unimodal taxa response curve. On average, the 2000 km radius leads to the use of 1165 modern samples with a T_{Jul} range of 21.6 K and an MI range of 2.08 m/m.

WAPLS is a well-established reconstruction method that has performed competitive with other statistical techniques, including response surfaces, boosted regression trees, neural networks, and Bayesian techniques, in a wide range of applications (e.g Salonen et al., 2019; Tipton et al., 2019). Compared to the often-used modern analog technique, estimates suffer less from auto-correlation in the calibration data and are more robust for non-analog vegetation compositions which are typical for glacial climates (e.g. Chevalier et al., 2020). Unlike indicator taxa methods, which only use information on the occurrence of taxa, WAPLS exploits the information on varying abundances of taxa over time. Reconstructions from inverting vegetation models are sensitive to the employed model and its climate-CO_2-vegetation

relationship. In addition, taxa need to be mapped to PFTs or biomes in these approaches which is sometimes ambiguous and looses information on the climate ranges of individual taxa. Thus, WAPLS has advantages over several other techniques for reconstructing the Siberian LGM climate, whereas no other established technique is clearly superior to WAPLS. To overcome the ignorance of lower CO_2 concentrations by the WAPLS method, we apply an a posteriori correction described below.

Climate reconstructions from statistical transfer functions can be biased if the signal of a dominant environmental variable superimposes the reconstructed variable (Juggins, 2013; Rehfeld et al., 2016). Therefore, the selection of identifiable variables needs to be examined statistically and using expert elicitation (Salonen et al., 2019). Previous authors interpreted Central and Eastern Siberian pollen records mainly as recorders of summer temperature and aridity (e.g. Alfimov and Berman, 2001; Kienast et al., 2005; Sher et al., 2005; Wetterich et al., 2011; Ashastina et al., 2018). Therefore, we use T_{Jul} as a measure of summer temperature and MI as a measure of moisture availability. In addition, we compute reconstructions for T_{ann} which are required for the a posteriori correction for lower CO_2 concentrations. We evaluate the statistical performance of the transfer functions using the coefficient of determination between observed and predicted variables in the calibration data (R^2), the bootstrapped root mean square error of prediction in the calibration data (RMSEP), and the significance test of Telford and Birks (2011), which compares the explained variance in the fossil data against randomized transfer functions. In these tests, all three variables perform comparable. We select T_{Jul} and MI for the state estimates as they have been identified by previous studies as most important limiting factors of plant growth in Siberia.

3.1.2 Correcting statistical reconstructions for lower CO_2 concentrations

The calibration of the statistical transfer functions with modern pollen and climate data implicitly assumes that confounding environmental variables do not change over time or that the changes do not influence the relationship between the pollen assemblages and the reconstructed climate variable. During the LGM, CO_2 concentrations were much lower such that more water is needed to assimilate the same amount of carbon. This reduced water use efficiency can lead to biases as environmental conditions appear dryer than the were in reality. Theoretical considerations (Williams et al., 2000; Prentice et al., 2017) and previous reconstructions with vegetation models for Northern Eurasia, North America, and China (Wu et al., 2007a; Izumi and Bartlein, 2016; Wu et al., 2019) suggest that the influence of changing CO_2 concentrations on reconstructions of seasonal temperatures is small compared to other sources of uncertainty in the reconstructions. Therefore, we focus in the following on the influence of CO_2 changes on MI reconstructions.

To correct the statistical MI reconstructions for lower CO_2 concentrations during the LGM, we apply a recently developed a posteriori method which infers water use efficiency from MI, T_{ann}, and CO_2 concentration (Prentice et al., 2017; Cleator et al., 2020; Wei et al., 2021) based on a global model for carbon uptake (Prentice et al., 2014; Wang et al., 2017). An optimality approach connects the reconstructed temperature, statistically reconstructed MI, and modern CO_2 level with the modern temperature, actual past MI, and past CO_2 level. The method is described in Wei et al. (2021) and Prentice et al. (2017). To determine the correction factor for MI, we use the WAPLS reconstructions of MI and T_{ann} together with the modern climatologies, and average CO_2 concentrations for the period 19-23ka from Köhler et al. (2017). As modern CO_2 concentrations, we use 334.3 ppm which is the mean value for the period 1950-2000 CE in Köhler et al. (2017). The computed correction factor is added to the WAPLS-based MI reconstruction. To account for uncertainties in the T_{ann} reconstruction, we sample T_{ann} from the mean reconstruction and bootstrapped RMSEP.

3.2 State estimates

The state estimate framework is adapted from Weitzel et al. (2019). The strategy is to use a climate simulation ensemble for spatial interpolation and structural extrapolation of the local climate reconstructions from the pollen samples. An additional residual stochastic field accounts for structural differences between the simulations and pollen-based reconstructions. We use Bayesian hierarchical modeling

to combine modules for the proxy-climate relationship (data stage), the spatial interpolation (process stage), and the estimation of additional model parameters (prior stage). Uncertainties from the local reconstructions, the simulation ensemble, and the model parameters are naturally propagated through the inference process. Using Bayes theorem, the so-called posterior probability of the Siberian LGM climate C_p and estimated model parameters θ, ϑ, and ω, i.e. the probability of C_p and the parameters given the proxy data P and the simulation ensemble $M_1, ..., M_{12}$ is proportional to:

$$\underbrace{\mathbb{P}\left(C_p, \theta, \vartheta, \omega \mid P, M_1, ..., M_{12}\right)}_{\text{Posterior}} \propto \underbrace{\mathbb{P}\left(P \mid C_p, \theta\right)}_{\text{Data stage}} \underbrace{\mathbb{P}\left(C_p \mid \vartheta, \omega, M_1, ..., M_{12}\right)}_{\text{Process stage}} \underbrace{\mathbb{P}\left(\theta\right) \mathbb{P}\left(\vartheta\right) \mathbb{P}\left(\omega\right)}_{\text{Prior stage}}. \quad (2)$$

Here, θ are transfer function parameters, ϑ are parameters of the residual stochastic field, and ω are weights estimated for the ensemble members to optimize the fit between reconstructions and simulations.

The data stage models the incorporation of the information from the local reconstructions using a Gaussian observation model. The best estimates from the transfer functions are employed as data and the bootstrapped RMSEPs, propagated through the CO_2 correction algorithm via Monte Carlo sampling, as standard deviations of each proxy sample. The samples influence the state estimate in other grid boxes only through the spatial interpolation. Part of the transfer function uncertainty is shared among samples from the same record, for example uncertainties related to the modern calibration dataset. Therefore, we introduce a correlation parameter which estimates the shared fraction of the uncertainty. As the WAPLS transfer functions do not provide information on the fraction of dependent uncertainty, this parameter is fitted during the inference process.

Comparing several formulations of the process stage, Weitzel et al. (2019) recommend using a multivariate Gaussian distribution with additional parameters constrained by proxies. As in Weitzel et al. (2019), the mean of the Gaussian distribution is given by a weighted mean of the ensemble members with weights estimated from the local reconstructions. This gives more importance to ensemble members that fit better to the proxy data. The spatial covariance matrix models the residual deviation between weighted ensemble mean and local reconstructions. Due to the limited number of proxy records, complex matrix formulations are unidentifiable from the data. We use a Matérn covariance matrix with smoothness parameter 3/2 which corresponds to a diffusive transport of a white noise energy input (Whittle, 1963). We employ the Gaussian Markov random field approximation of Lindgren et al. (2011) to speed up computations through a sparse inverse covariance matrix. The covariance matrix is defined by three parameters, the amplitude of the variance, the spatial decorrelation length, and the anisotropy, which are fitted during the inference process.

The prior stage in Eq. (2) contains prior distributions of the parameters θ, ϑ, and ω which ensure that the posterior distribution is a valid probability distribution. We employ weakly informative prior distributions (see Online Resource 1 for details).

We infer the posterior distribution using a Markov chain Monte Carlo algorithm which combines Gibbs sampling for C_p with Metropolis-Hastings updates for θ, ϑ, and ω. The state estimation framework and inference strategy are described in detail in Online Resource 1.

4 Results

In this section, we first present results from the local reconstructions, including the spatial pattern of reconstructions, the transfer functions performance, and the influence from applying the CO_2 correction algorithm to the MI reconstructions. Then, we show the state estimates, which combine the local reconstructions with the simulation ensemble. We analyze the T_{Jul} and the MI posterior distributions, before showing how the ensemble member weights ω can be used to study which atmospheric conditions lead to a good fit with the local reconstructions.

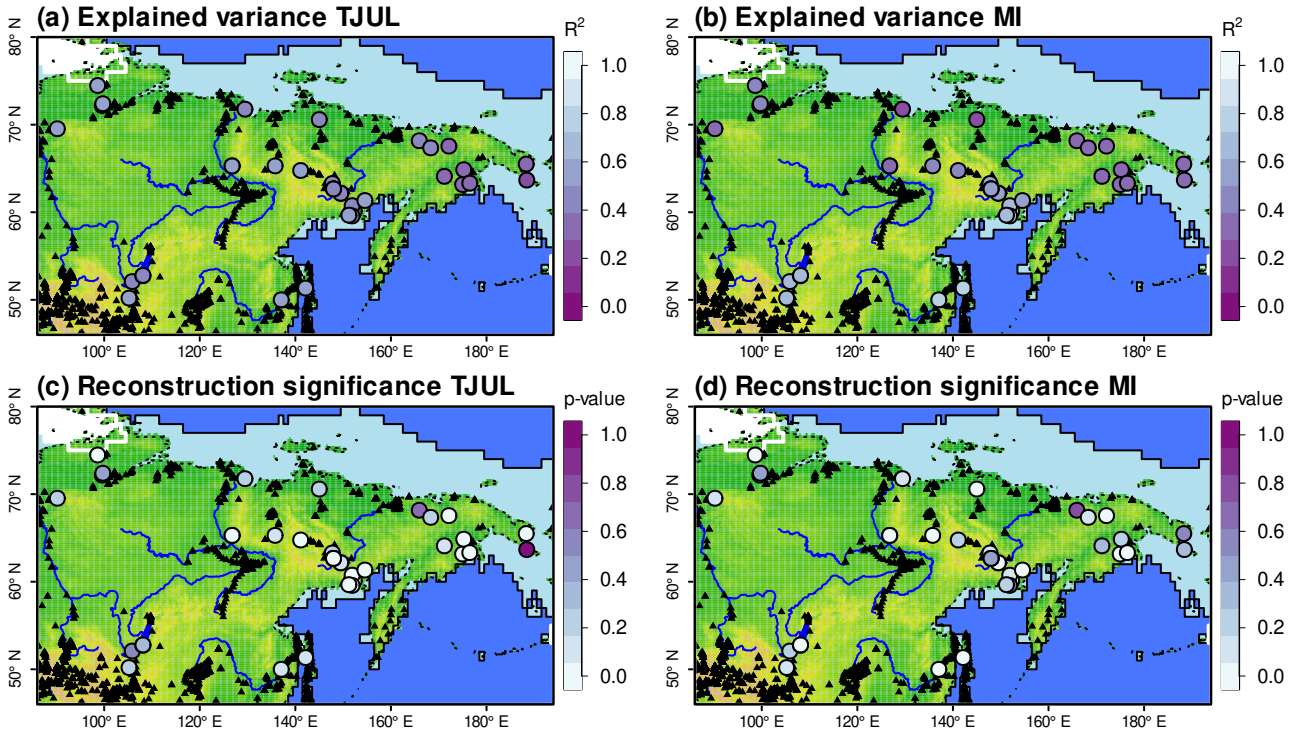

Figure 4: Performance statistics of the WAPLS transfer functions (colored dots), (a) explained variance (R^2) of T_{Jul}, (b) explained variance (R^2) of MI, (c) significance of T_{Jul} reconstruction (p-value), (d) significance of MI reconstruction (p-value). Modern samples are shown as black triangles. The LGM coastline is denoted by thick black lines, the modern coastline by dotted lines, major rivers by blue lines, and the PMIP3 LGM ice sheet extent by a white line.

4.1 Local reconstructions

4.1.1 Spatial patterns

Fig. 2 shows the pollen-based reconstructions and their uncertainties together with summary statistics of the simulation ensemble. In the figure, we average the WAPLS estimates of the samples in the period 19-23ka for each record. On average, the record mean anomaly from present-day is −0.4 K but with a spread ranging from anomalies of −5.7 K to +6.6 K. The highest anomalies, with often higher LGM temperature than today, occur along the modern Arctic Ocean coastline. On average slightly negative anomalies are present along the Pacific Ocean coastline. The lowest anomalies occur in more continental areas, e.g. in the Yana region and near Lake Baikal. The reconstructions tend to feature higher anomalies than the model ensemble mean (Fig. 2a).

Reconstructed MI is on overage similar to present day values with a mean record anomaly of +0.09 m/m after correcting for the lower CO_2 concentration. Record anomalies range from −0.71 m/m to +0.50 m/m. The lowest anomalies occur at the Bering Strait, which was closed during the LGM. MI values are similar to or slightly higher than present-day values along the Pacific and Arctic Ocean coastlines. There is a reasonable agreement between reconstructions and simulation ensemble mean (Fig. 2b), except in the region between Lena and Kolyma, where the reconstructions indicate an overall wetting (locally up to +0.4 m/m), whereas a mean drying is simulated (locally up to −0.35 m/m). In records with high temporal resolution, we find mostly small inter-sample variations during the 19-23ka time slice (see Online Resource 1). This supports the notion of a relatively stationary climate within this period. We exploit this finding in the state estimate below by including all samples without explicitly modelling temporal variations.

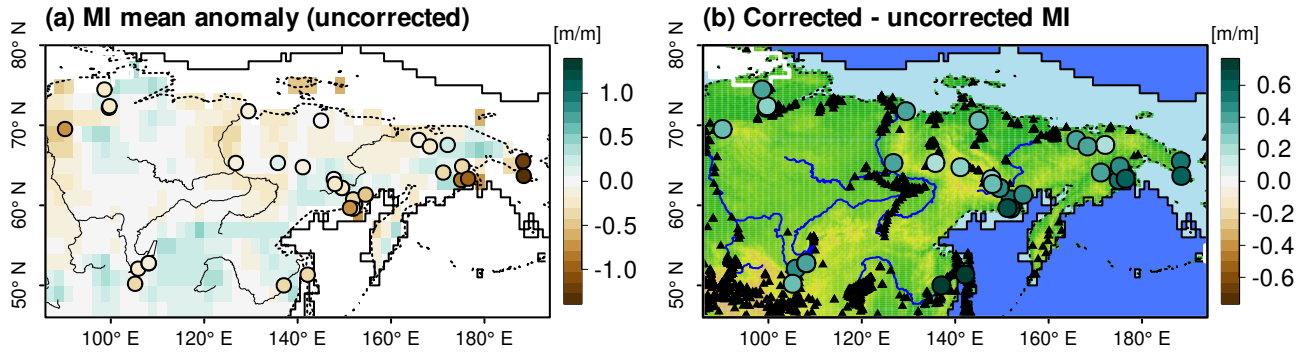

Figure 5: Influence of CO_2 concentration on local MI reconstructions. (a) Same as Fig. 2b but for local MI reconstructions without applying the CO_2 correction. (b) Difference between CO_2 corrected and uncorrected local MI reconstructions (colored dots), modern samples are shown by black dots. The LGM coastline is denoted by thick black lines, the modern coastline by dotted lines, major rivers by thin black lines, and the PMIP3 LGM ice sheet extent by a white line.

4.1.2 Reconstruction uncertainties and transfer function performance

The reconstruction uncertainties, quantified by the bootstrapped RMSEP from the WAPLS transfer functions, propagated through the CO_2 correction algorithm for MI reconstructions, are mostly smaller than the simulation ensemble standard deviation (Fig. 2c,d). The mean uncertainties are 2.6 K for T_{Jul} and 0.31 m/m for MI. The T_{Jul} values are consistent across the domain except for larger uncertainties in the Baikal region. The latter might originate from large climatic ranges as the 2000 km radius reaches into Northern China for these records. For MI, the uncertainties show low spatial heterogeneity.

The explained variance R^2 between predicted and observed values in the modern training set is comparable for T_{Jul} (mean $R^2 = 0.46$) and MI (mean $R^2 = 0.49$). The spread of R^2 values is small with a standard deviation of 0.09 for T_{Jul} and 0.16 for MI. Spatial gradients for T_{Jul} are generally small (Fig. 4). A slight north-south gradient is apparent for MI with higher explained variance in the Southern than in the Northern part of the reconstruction domain (Fig. 4).

The median p-values in the significance test are 0.10 for T_{Jul} and 0.06 for MI. This means that for both variables around half of the records perform better than at least 90% of randomized transfer functions. Additionally, 69% of records for T_{Jul} and 75% for MI have a p-value below 0.25. These results show that both variables perform significantly better than expected for randomized transfer functions and thus explain important parts of the ecological changes recorded in the records. The p-values of T_{Jul} are particularly low in Eastern Siberia, whereas the spatial heterogeneity of p-values is small for MI (Fig. 4).

The significance test statistics are on average better than in the Northern Hemisphere reconstructions by Herzschuh et al. (2022a), which include North America, Europe, and Asia. It should be noted that this might be in parts due to including a larger signal from the glacial-interglacial transition in the records used here, whereas the Northern Hemisphere dataset is also containing records covering only the Holocene. The generally good performance is encouraging as Siberia is still under-sampled with modern pollen samples compared to Europe, North America, and China. This shows that the modern data is covering a sufficient environmental range to explain past pollen variations. Different taxa respond sensitive to T_{Jul} than to MI. This leads to a low correlation of T_{Jul} and MI reconstructions (cor=0.02) as well as there respective performance statistics (cor=0.30 for p-values, cor=0.51 for R^2). These results increase the confidence that the reconstructions are not substantially biased by correlations between explanatory variables in the modern calibration data.

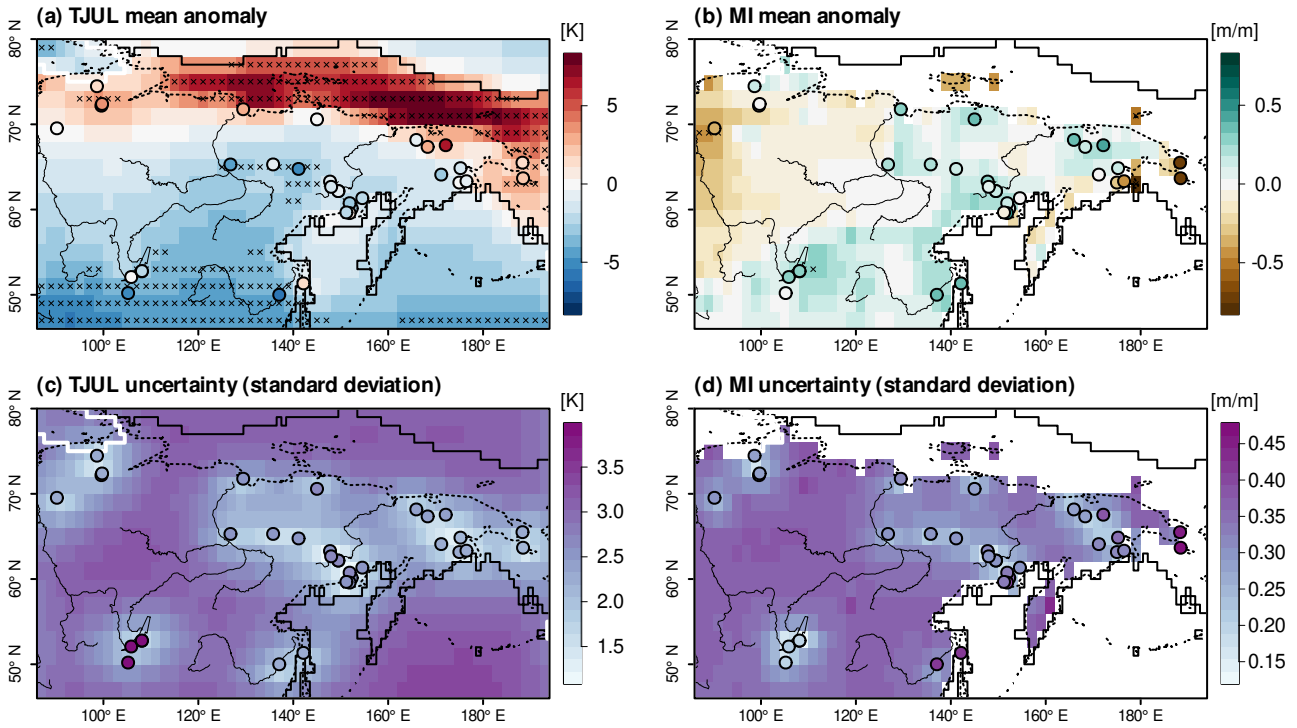

Figure 6: Summary statistics of state estimates, (a) T_{Jul} posterior mean anomaly, (b) MI posterior mean anomaly, (c) T_{Jul} posterior standard deviation, (d) MI posterior standard deviation. Colored dots depict local reconstructions. In the top row, grid box-wise significant anomalies (p ¡ 0.1) are marked by black crosses. The LGM coastline is denoted by thick black lines, the modern coastline by dotted lines, major rivers by thin black lines, and the PMIP3 LGM ice sheet extent by a white line.

4.1.3 Influence of CO_2 correction

To diagnose the influence of the a posteriori correction of MI reconstructions for lower CO_2 values, we show the uncorrected reconstructions in Fig. 5 together with the difference of corrected and uncorrected values. The mean anomaly over all uncorrected reconstructions is -0.35 m/m which indicates a substantial drying compared to present-day. The reconstructions with the most negative anomalies occur along the Pacific Ocean coastline where also the influence of the CO_2 correction is largest. The mean MI anomaly correction of $+0.44$ m/m suggests that a large amount of the perceived drying diagnosed from comparing past and modern pollen can be attributed to the lower CO_2 levels. This strong influence of CO_2 on glacial-interglacial vegetation changes in Siberia is in agreement with model simulations (Harrison and Prentice, 2003; O'ishi and Abe-Ouchi, 2013).

4.2 State estimates

4.2.1 July temperature

Averaged over the reconstruction domain, the mean T_{Jul} anomaly of the state estimate is -1.4 K with a standard deviation of 0.7 K. This spatial average is the result of a south-west to north-east gradient with anomalies around -5 K in the Baikal and Amur region, T_{Jul} similar to present-day along the modern Arctic Ocean and Sea of Okhotsk coastlines and up to $+8$ K higher temperatures on the Siberian shelf and the Bering Strait which were land regions during the LGM (Fig. 6a). The high anomalies over the Siberian shelf are an extrapolation as simulations with temperatures near present-day values along the modern coastline feature substantially positive anomalies over the Siberian shelf. Negative anomalies in the southeastern part of the domain and positive anomalies over the Siberian Shelf and Bering Strait are mostly significant on a $p < 0.1$ level. In Central and Eastern Siberia, significant anomalies ($p < 0.1$)

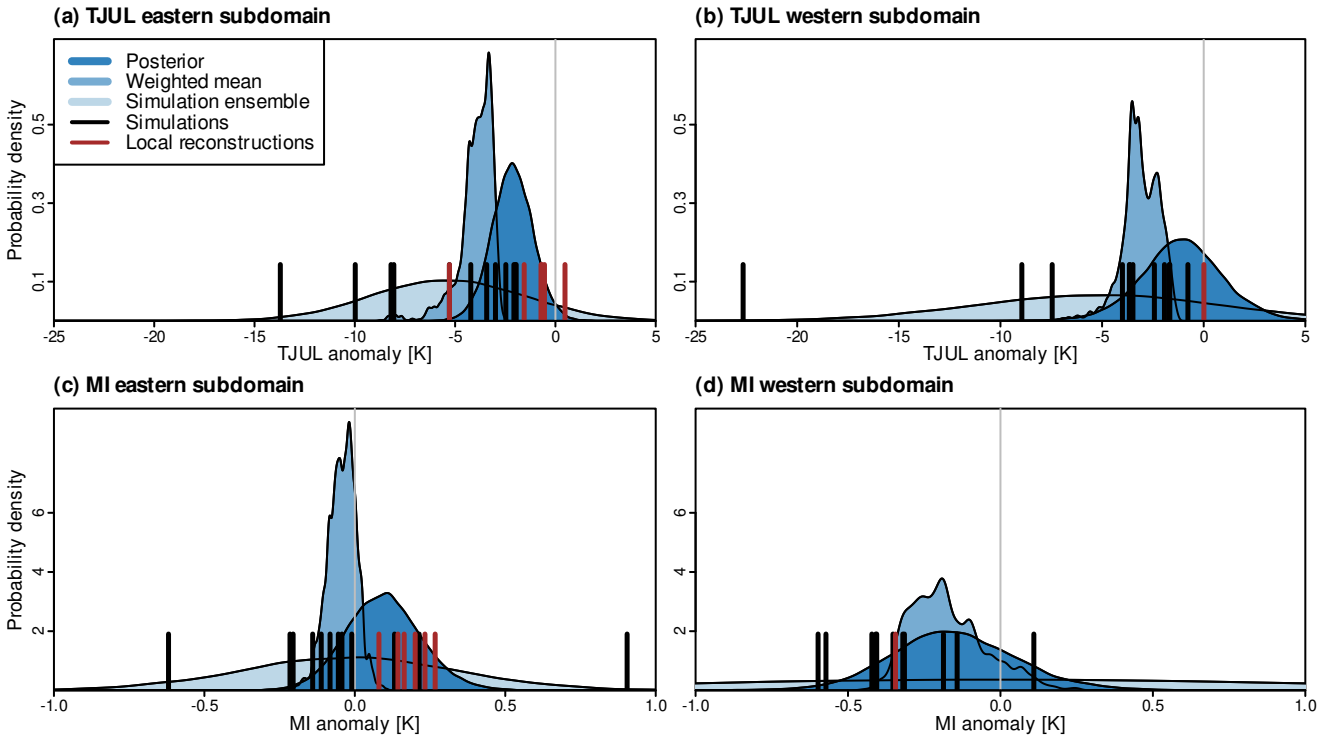

Figure 7: Effect of the proxy data on the unconstrained simulation ensemble. Posterior (dark blue), posterior weighted ensemble means (blue), and Gaussian approximation of simulation ensemble (light blue) probability densities of (a) T_{Jul} averages in the eastern subdomain, (b) T_{Jul} averages in the western subdomain, (c) MI averages in the eastern subdomain, (d) MI averages in the western subdomain. The black bars denote anomalies of the ensemble members, the brown bars are local reconstruction means for proxy records in the domain. The eastern region is better covered by proxy data leading to more precise posterior estimates, while the western region is strongly affected by one ensemble member outlier. See Fig.1 for the area definition.

are featured only for a few grid boxes with strong proxy constraints.

With posterior standard deviations of 1-2 K, uncertainties are lowest in areas with strong proxy constraints, particularly Eastern Siberia and the Taymyr Peninsula (Fig. 6c). Standard deviations rise up to 4 K in the region between Lake Baikal, Taymyr Peninsula and Lena due to a high ensemble spread and weak proxy constraints. Despite adding a residual stochastic field, the posterior uncertainties are substantially lower in most regions than the standard deviation of the simulation ensemble (compare Fig. 2 and 6).

The effect of proxy data on the posterior distribution is demonstrated by comparing two subdomains (rectangles in Fig. 1). In both regions, the posterior mean is higher than the ensemble mean and the posterior distribution is narrower than a Gaussian approximation of the ensemble (Fig. 7). The temperature increase from the prior to the posterior is decomposed into higher weights for simulations with higher anomalies and an additional increase from the residual stochastic field (Fig. 7). The uncertainty in the distribution of weighted means is smaller than for the full posterior due to the omission of this residual stochastic field. The posterior uncertainty in the eastern subdomain is much smaller than in the western subdomain because of more nearby proxy records and a smaller simulation ensemble spread.

4.2.2 Moisture index

Similar to local reconstruction and ensemble mean, the area-averaged mean anomaly of the state estimate is nearly zero (+0.01 m/m), with a standard deviation of 0.08 m/m. Following the pattern of the local reconstructions, the posterior mean shows a west to east gradient, with negative anomalies in

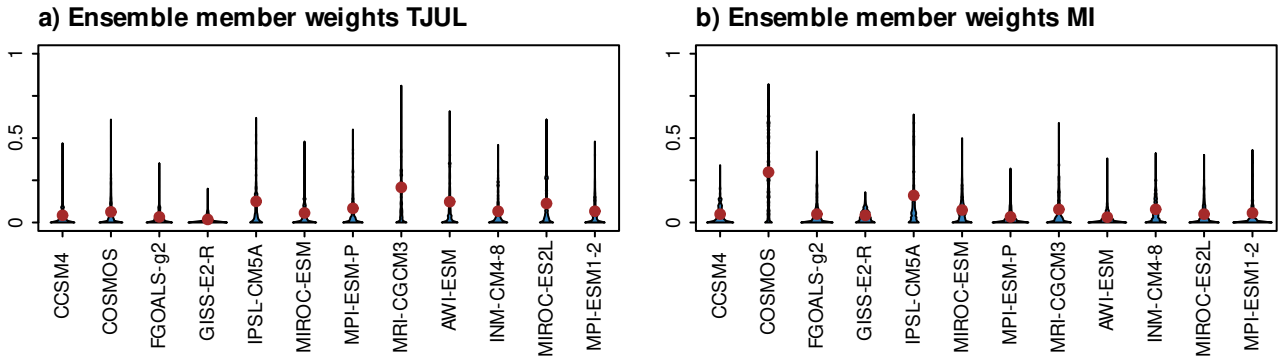

Figure 8: Posterior distributions of ensemble member weights for (a) T_{Jul} and (b) MI. Posterior means are shown as brown dots.

the Jenissei region, values similar to today in the Lena region, and slightly positive anomalies (up to $\sim +0.3$ m/m) in Eastern Siberia and in a band from Lake Baikal to the Amur river. Along the Bering Strait, posterior mean anomalies are negative. Almost no grid boxes exhibit significant anomalies ($p < 0.1$). Reconstruction uncertainties are lowest in areas with nearby proxy records unless the the uncertainty in the pollen-based reconstructions is very high, e.g. at the Bering Strait and in the Amur region. The lowest uncertainties occur around Lake Baikal with standard deviations of ~ 0.15 m/m, whereas standard deviations grow to ~ 0.4 m/m in the region between Taymyr Peninsula, Lake Baikal and Lena.

Similar to the T_{Jul} reconstruction, we see strongly decreased posterior uncertainties in the eastern and western subdomains compared to a Gaussian approximation of the simulation ensemble. The posterior means are relatively close to the ensemble means and the weighted ensemble means. The stronger proxy constraints in the eastern subdomain lead to smaller posterior uncertainties compared to the western subdomain.

4.2.3 Ensemble member weights

To account for the large ensemble spread, our reconstruction framework estimates weighted means that fit best with the local reconstructions. Due to the uncertainties in the local reconstructions, these posterior weights are again probability distributions. We exploit the weights to analyze climatic processes that can potentially explain the diagnosed LGM state. For the T_{Jul} reconstruction, highest posterior weights are obtained by the MRI-CGCM3 simulation (mean weight of 0.21), followed by the IPSL-CM5A, AWI-ESM, and MIROC-ES2L simulations (Fig. 8a). All of these simulation are among the ensemble members with highest anomalies (Table 2). In contrast, GISS-E2-R, FGOALS-g2, and CCSM4, which are among the ensemble members with lowest anomalies, feature the lowest weights.

Fig. 9 shows the difference between posterior weighted means, i.e. with weights given by the posterior mean of the T_{Jul} reconstruction (Fig. 8), and equally weighted ensemble means for several variables. The posterior weighted mean T_{Jul} is up to +3 K higher in Northern Siberia but barely higher than the ensemble mean outside of Northern Eurasia (Fig. 9a). The summer precipitation difference between the posterior and equally weighted means are very small suggesting that the anomalous temperatures are not associated with precipitation anomalies (Fig. 9b). The posterior weighted means feature higher 500 hPa geopotential height anomalies, reduced cloud cover over Northern Siberia, weaker eastward zonal wind, and anomalous meridional flow patterns over Eurasia.

For MI, reconstructions close to the ensemble mean are given highest weights, in particular COSMOS-ASO (mean weight 0.30) and IPSL-CM5A (Fig. 8b). The differences between the MI posterior weighted and the equally weighted means of the same variables than described above are smaller than for the weights deduced from the T_{Jul} reconstruction, but the patterns tend to be similar between the two reconstruction variables (see Online Resource 1).

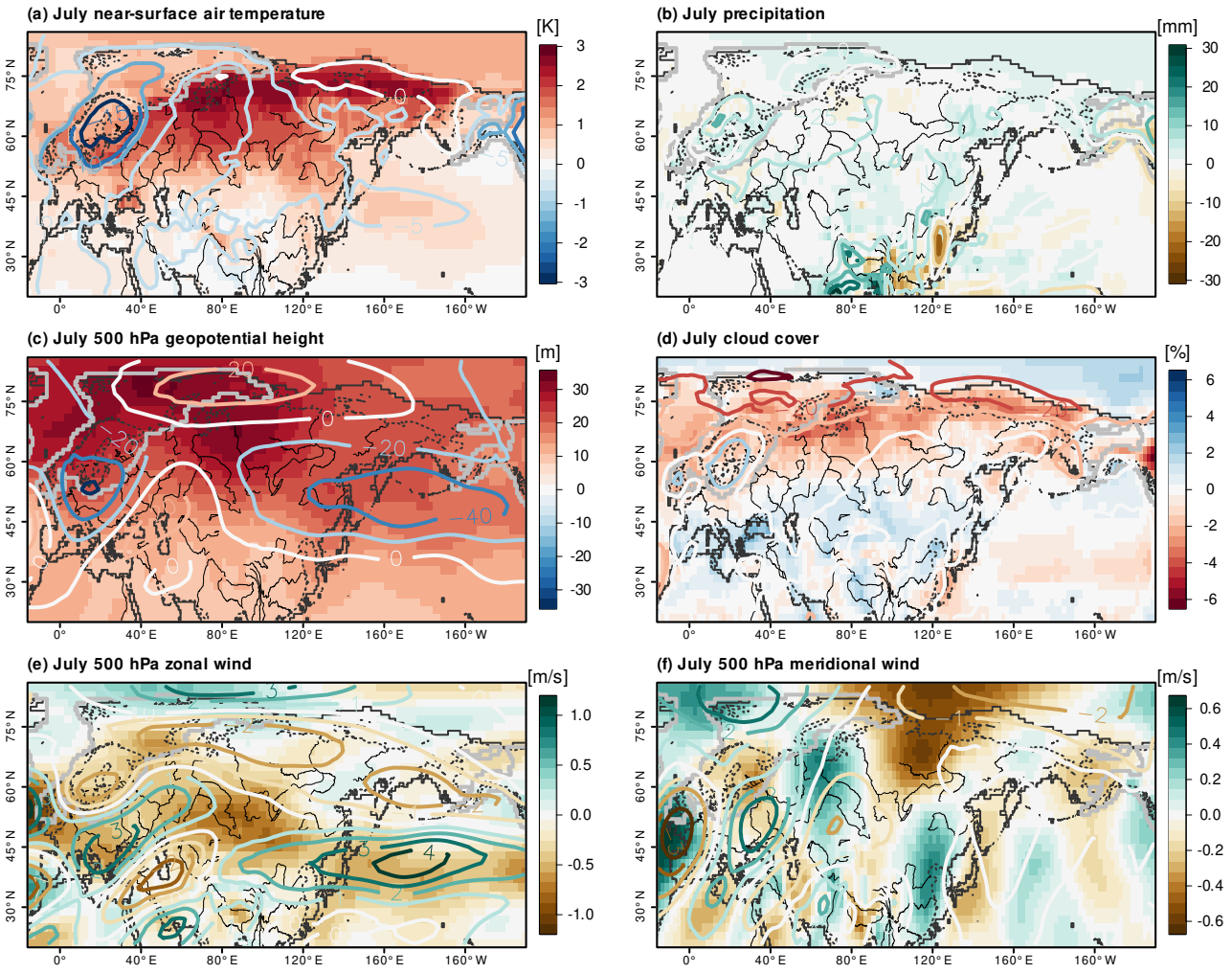

Figure 9: Posterior weighted ensemble means minus equally weighted ensemble means for a) T_{Jul}, b) July precipitation, c) July 500hPa geopotential height, d) July cloud cover, e) July 500hPa zonal wind, f) July 500 hPa meridional wind. Posterior weights are given by the mean ensemble member weights of the T_{July} state estimate. Contours show the LGM anomaly of the equally weighted ensemble means. The LGM coastline is denoted by thick black lines, the modern coastline by dotted lines, major rivers by thin black lines, and the PMIP3 LGM ice sheet extent by a white line.

5 Discussion

Our reconstructions show higher Siberian T_{Jul} LGM anomalies than in most high-latitude regions, and MI values similar to present-day. The latter is a result from applying an a posterior correction to the WAPLS estimates, which shows that a perceived drying deduced from comparing past and modern pollen can be explained mostly by the plant-physiological effects from lower CO_2 concentrations. Analyzing posterior weighted ensemble means, we find that best-fitting model combinations are associated with higher temperature anomalies in Northern Siberia, reduced cloud cover and anomalous atmospheric circulation patterns compared to the equally weighted ensemble mean. In the following, we compare our new state estimates with previous studies. Then, we discuss implications of our results for the Siberian LGM climate as well as potential limitations of our study and recommendations for future reasearch.

5.1 Comparison with previous work

Here, we compare our results with previous summer temperature, T_{ann}, and moisture availability reconstructions for Siberia as well as sea surface temperature (SST) reconstructions for the Northwestern Pacific. Previous studies of the Siberian LGM climate are of quantitative or qualitative nature. Therefore, we classify them in broad categories. A comparison with our reconstructions is provided in Table 3. Averaged over the reconstruction domain, the T_{ann} state estimates of Tierney et al. (2020) and Annan and Hargreaves (2013) are much colder than our T_{Jul} estimate with mean anomalies of -6.7 K and -5.2 K, respectively. This difference could be explained by a strong increase in seasonality, the absence of proxy reconstructions in Central and Eastern Siberia in these state estimates, or the lower temperature simulation ensemble employed by Tierney et al. (2020).

The pollen-based reconstructions by Tarasov et al. (1999), Wu et al. (2007a), and Cleator et al. (2020) are mostly limited to Western Siberia and thus west of our reconstruction domain. However, they support our finding for Central Siberia of higher summer temperature anomalies in high than mid-latitudes. In the Jenissei region, these three studies feature summer temperatures similar to present-day, which agrees with our state estimate (Table 3). The borehole-based T_{ann} LGM anomaly of ~ -4 K from Dorofeeva et al. (2002) for Lake Baikal and estimates of -1 K to -5 K from the pollen records in the same region by Tarasov et al. (1999) are comparable to our posterior mean of -3.4 K for the Baikal region (Table 3, see Fig. S9 in Online Resource 1 for definitions of the regions). This value is in good agreement with the -3.8 K anomaly for the Baikal region in the state estimate by Cleator et al. (2020). The summer temperatures in Wu et al. (2007a) are closer to present-day values than in our study, Tarasov et al. (1999), and Cleator et al. (2020) but with considerable spatial heterogeneity between the sites. This difference might originate from the difference in the reconstruction method (inverse modeling versus statistical transfer functions) or slight negative biases from not correcting for lower CO_2 levels.

The complex anomaly pattern of our reconstruction in Central Siberia and along the Arctic Ocean is reflected in previous work. In the Yana region, we reconstruct moderately negative T_{Jul} anomalies. This is in agreement with pollen and macrofossil analyses by Pitul'Ko et al. (2007) and Ashastina et al. (2018). While Andreev et al. (2011) infers lower summer temperatures along the Arctic Ocean from pollen records, Kienast et al. (2005) (macrofossils) and Sher et al. (2005) (pollen, faunal remains) find higher or slightly lower summer temperatures in the Lena Delta. Our estimates of small T_{Jul} anomalies in the Lena delta support the latter results.

For Eastern Siberia, reconstructed positive T_{Jul} anomalies from fossil insect assemblages by Berman et al. (2011) for the Kolyma region, estimates between -4 K and +3 K by Alfimov and Berman (2001) (fossil insects), and summer temperatures similar to present-day on Kamchatka Peninsula inferred from biomarkers by Meyer et al. (2017) are within the uncertainty ranges of our reconstruction. The strongly positive anomaly for Ayon Island reconstructed by Alfimov and Berman (2001) supports our finding of positive anomalies on the Siberian shelf in summer due to the lower sea level. Our reconstruction anomalies are higher than the pollen-based reconstruction by Lozhkin et al. (2007) for El'gygytgyn Lake.

For the Northwest Pacific and the Sea of Okhotsk, the inferred summer SST anomalies of around -1.5 K by Kiefer et al. (2001) (foraminifera assemblages) and Meyer et al. (2016) (TEX86), and -3 K by Seki et al. (2009) (TEX86) are within the uncertainties of our estimate (-2.3 ± 1.9 K). Similar to

Table 3: Comparison of our reconstructions with previous work based on five subdomains. For our reconstructions, we show the spatial mean anomalies and standard deviations from the state estimates. To homogenize the T_{Jul} estimates from other studies, we aggregate them in qualitative categories. For definitions of subdomains and translations of quantitative temperature reconstructions into qualitative characterizations (where available) see Online Resource 1. For the Jenissei region, we aggregate estimates from Tarasov et al. (1999); Wu et al. (2007a); Cleator et al. (2020); for Lake Baikal from Tarasov et al. (1999); Dorofeeva et al. (2002); Wu et al. (2007a); Cleator et al. (2020); for Arctic Ocean and Yana from Kienast et al. (2005); Sher et al. (2005); Pitul'Ko et al. (2007); Andreev et al. (2011); Ashastina et al. (2018); for Eastern Siberia from Alfimov and Berman (2001); Berman et al. (2011); and for Pacific from Kiefer et al. (2001); Seki et al. (2009); MARGO Project Members (2009); Meyer et al. (2016, 2017); Meyer and Barr (2017).

Region	Mean T_{Jul} [K]	Std. dev. T_{Jul} [K]	Literature estimates summer temperature	Mean MI [m/m]	Std. dev. MI [m/m]	Literature hydroclimate
Jenissei	+0.1	1.7	Similar	-0.43	0.25	Dryer
Lake Baikal	-3.4	1.6	Moderately lower to similar	+0.05	0.14	Dryer to similar
Arctic Ocean and Yana	+0.7	1.3	Moderately lower to slightly higher	+0.07	0.16	Dryer
Eastern Siberia	+0.2	0.8	Substantially lower to slightly higher	+0.02	0.11	
Pacific	-2.3	1.9	Moderately lower to similar	-0.05	0.29	Similar

MARGO Project Members (2009), our reconstruction features rising temperature anomalies from south to north in the North Pacific.

To conclude, the spatial summer temperature patterns emerging from the literature review are reflected in our reconstruction. However, some of the lowest reported anomalies are outside of our uncertainty estimates. This is perhaps due to the smoothing effect of the spatial interpolation which is not present in previous studies.

Consistently dryer conditions during the LGM inferred from pollen and plant macrofossils by previous studies (e.g. Tarasov et al., 1999; Sher et al., 2005; Pitul'Ko et al., 2007; Lozhkin et al., 2007; Wu et al., 2007a; Andreev et al., 2011; Ashastina et al., 2018; Cleator et al., 2020) are in agreement with the local MI reconstructions when not correcting for the lower CO_2 concentrations. However, the corrected MI values are mostly wetter than previous estimates. As most previous studies have not separated reduced moisture availability from lower CO_2 concentration effects, a direct comparison with our estimates is only possible for the studies by Wu et al. (2007a) and Cleator et al. (2020). Our MI estimates for the Jenissei region are in agreement with the reduced moisture availability reconstructed from pollen sequences by Tarasov et al. (1999), Wu et al. (2007a), and Cleator et al. (2020), although the magnitude of MI reduction is larger in Cleator et al. (2020) than in our reconstruction (-1.10 m/m compared to -0.43 m/m). For the Baikal region, our MI anomaly ($+0.05 \pm 0.14$ m/m) is higher than the Cleator et al. (2020) state estimate (mean of -0.22 m/m), whereas the actual over potential evapotranspiration anomalies by Tarasov et al. (1999) range from -22% to $+22\%$ in accordance with our state estimate. Wu et al. (2007a) reconstructs slightly negative actual over potential evapotranspiration anomalies, which are still within the uncertainty ranges of our reconstruction. Thus, we find similar spatial gradients between the Jenissei and Baikal regions than Tarasov et al. (1999), Wu et al. (2007a), and Cleator et al. (2020). However, further work is needed to explain the lower MI anomalies in Cleator et al. (2020) compared to our state estimate.

5.2 Implications for the Siberian LGM climate

Our reconstructions provide evidence for higher LGM summer temperature anomalies in Siberia compared to other high-latitude regions and moisture availability similar to present-day levels. As noted previously (Bakker et al., 2020), LGM simulations have a wide ensemble spread for summer temperature over Siberia. Our state estimate anomaly is comparable to the cluster of PMIP3 and PMIP4 simulations with the highest summer temperature anomalies. Interestingly, the spread of the four PMIP4 simula-

tions in our ensemble is smaller than in the PMIP3 simulations (see Table 2). This might be due to the smaller number of simulations, changes in boundary conditions from PMIP3 to PMIP4, or changes in model formulation. All PMIP4 simulations are in the high temperature anomaly cluster and thus suggest improved representation of Siberian summer temperatures compared to PMIP3. However, the simulations with the highest posterior weights are still from PMIP3 for T_{Jul} and MI.

There is a substantial wetting effect from correcting the MI reconstructions for lower CO_2 concentrations, which shifts the local reconstructions from a mean drying to very small changes. This wetting effect is in concordance with inverse modelling studies (Wu et al., 2007a; Izumi and Bartlein, 2016; Wu et al., 2019). In these studies, small effects from CO_2 on pollen-based temperature reconstructions were found for Northern Eurasia, North America, and China. Other studies suggest reconstruction biases towards lower temperatures due to lower CO_2 concentrations, albeit not explicitly for Northern Eurasia (Cowling and Sykes, 1999; Wu et al., 2007b). The latter would imply even higher T_{Jul} anomalies than reconstructed here. Thus, the two main findings from our T_{Jul} reconstruction summarized above would be further strengthened. Another argument against significant biases in our T_{Jul} state estimate is the agreement with vegetation-independent (e.g. fossil insects, biomarkers, geochemical indices) summer temperature reconstructions for Northern Siberia, the Sea of Okhotsk, and the North Pacific discussed in Sect. 5.1. Since none of the proxies involved in these studies is expected to be biased by lower glacial CO_2 concentrations, they provide independent evidence for our inferred T_{Jul} ranges. Due to the uncertain effects of CO_2 changes on pollen-based reconstructions, we recommend further assessments of different modelling strategies to account for these.

The comparison of posterior weighted and equally weighted ensemble means provides insights into the mechanisms behind the reconstructed T_{Jul} and MI changes. Siberian temperature and precipitation changes are mostly decoupled in the simulations and higher temperatures in Siberia are a regional but not a global property (Table 2). Indeed, the posterior weighted means do not show substantially higher temperature anomalies outside of Northern Eurasia (Fig. 9a). The increased geopotential height anomaly in the posterior weighted mean is likely a direct consequence of the higher temperatures. Previous modelling studies showed a strong sensitivity of Siberian climate to ice sheet topographies through atmospheric circulation changes, in particular stationary wave patterns (Löfverström et al., 2014; Bakker et al., 2020). Our results support these findings, as the posterior weighted ensemble mean shows weakened eastward flow in the mid-latitudes and enhanced northward flow in Asia. These anomalous circulation patterns could lead to increased transport of warm air from Central and Eastern Asia to Siberia as suggested by Bakker et al. (2020). Similarly, local feedbacks such as the reduced cloud cover in the posterior weighted means might contribute to higher temperatures (Bakker et al., 2020).

The northward shift of the Arctic Ocean coastline has a strong effect on the surface heat capacity and energy balance. These changes should lead to increased seasonality on the Siberian shelf and nearby coastal areas, i.e. a stronger contrast between summer and winter temperatures. Such a change was also found for Western Siberia by Tarasov et al. (1999), Wu et al. (2007a), and Cleator et al. (2020), indicating that seasonality was stronger in large parts of Siberia. It would also reconcile our relatively high summer temperature estimates with findings of strong winter temperature decreases from isotopic compositions measured in ice wedges (Meyer et al., 2002; Wetterich et al., 2011; Opel et al., 2019; Wetterich et al., 2021), and the lower T_{ann} anomalies in the state estimates by Annan and Hargreaves (2013) and Tierney et al. (2020).

The physical mechanisms behind the absence of a large Siberian ice sheet during the LGM are still an open question. Previous studies suggest a combination of too high summer temperatures (e.g. Niu et al., 2019), too small precipitation amounts (e.g. Stauch and Gualtieri, 2008), or albedo effects from high dust levels (e.g. Krinner et al., 2006). Our results supports recent studies suggesting a dominant role of summer temperature (Meyer and Barr, 2017; Niu et al., 2019) as our reconstructions are in agreement with temperature anomalies preventing the growth of ice sheets in these studies. Our state estimate indicates that reduced precipitation and potential evapotranspiration balance each other, which leads to small MI changes. Independent proxies or theoretical constraints are needed to decompose the change in moisture availability into precipitation and evapotranspiration contributions. Further insights into the roles of temperature, precipitation, and dust could be gained by forcing ice sheet models with our

data-constrained estimates.

We suggest that future work should focus on closing the remaining data gaps in Central Siberia, where our state estimate is only weakly constrained by proxies. As pollen-based reconstruction are subject to various sources of uncertainties and potential biases (Birks et al., 2010; Chevalier et al., 2020), further vegetation-independent reconstructions (e.g. boreholes, geochemical tracers) are desirable for future research to evaluate our reconstructions.

6 Conclusions

We presented Last Glacial Maximum (LGM) climate state estimates from a new compilation of Central and Eastern Siberian pollen records with harmonized chronologies and taxonomy. Summer temperature (T_{jul}) and moisture availability (MI) are estimated with WAPLS transfer functions and an a posteriori method to correct the MI reconstructions for the lower CO_2 concentrations during the LGM. We combine the local reconstructions with a multi-model ensemble of PMIP3 and PMIP4 simulations for the LGM and infer the first gridded state estimate constrained by proxies from Central and Eastern Siberia.

Our reconstructions feature higher summer temperature anomalies than most high-latitude areas and moisture availability similar to present-day. The latter is likely due to balancing decreases in precipitation and potential evapotranspiration. The state estimate mostly follows the local reconstructions but with additional spatial smoothing. The posterior ensemble member weights from the reconstructions show that simulation combinations with higher LGM summer temperature anomalies than the ensemble mean and small changes in moisture availability in Siberia fit best with local reconstructions. A comparison of posterior weighted and equally weighted ensemble means shows that the anomalously high temperatures are a regional but not a global signal. High T_{jul} anomalies are associated with reduced cloud cover in Northern Siberia, weaker zonal flow in Eurasia, and increased northward flow in Central and Eastern Asia. Together with evidence from isotope compositions in ice wedges, our results suggest enhanced seasonality in Siberia during the LGM due to the northward shift of the Arctic Ocean coastline and anomalous atmospheric circulation patterns in response to the built-up of the Fennoscandian and Laurentide ice sheets.

The correction of MI reconstructions for lower CO_2 levels shows that a perceived drying diagnosed by the statistical transfer functions can be explained by the lower CO_2 levels. We do not apply correction factors to our temperature reconstructions. If these are biased low due to low CO_2 concentrations as some studies suggest, our conclusions on Siberian summer temperatures compared to other high latitude regions and the fit of simulations would be further strengthened. For future research, further method inter-comparisons would be valuable to assess the varying findings on the CO_2 influence on pollen-based reconstructions.

Our new state estimate is well-suited for future investigations of Siberian LGM climate. In particular, our results can provide new insights into the role of different climatic factors for the absence of a Siberian ice sheet during the LGM. Additionally, they could help to reconcile data and model-based findings on deglacial carbon fluxes in Siberia (Zech et al., 2011; Lindgren et al., 2018; Jeltsch-Thömmes et al., 2019) by providing more accurate atmospheric forcing to carbon cycle models.

Author contributions

Nils Weitzel, Ulrike Herzschuh, Andreas Hense, and Kira Rehfeld designed the study. Xianyong Cao and Thomas Böhmer computed the local reconstructions. Nils Weitzel implemented the CO_2 correction algorithm and the state estimation framework, and analyzed the data. All authors discussed the results. Nils Weitzel wrote the first version of the manuscript and all authors commented on previous versions of the manuscript. All authors read and approved the final manuscript.

Acknowledgements

NW and KR acknowledge funding by the Deutsche Forschungsgemeinschaft (DFG, German Research Foundation), project no. 395588486, and the Heidelberg Center for the Environment for providing a venue for discussion. NW

was additionally supported by the German Federal Ministry of Education and Research (BMBF) as Research for Sustainability initiative (FONA) through the PalMod project (FKZ: 01LP1509D). TB and UH acknowledge support from the Helmholtz Gemeinschaft and H2020 European Research Council project Glacial Legacy (Grant Number: 772852), and from the German Federal Ministry of Education and Research (BMBF) through the PalMod project (FKZ: 01LP1923B).

We thank Thomas Opel, Florian Kapp, Christian Ohlwein, and Jean-Philippe Baudouin for insightful discussions and comments on previous versions of the manuscript. We thank Sandy P. Harrison and Colin I. Prentice for help with the correction algorithm for lower CO_2 concentrations. We acknowledge all groups involved in producing and making available the PMIP3 and PMIP4 multi-model ensembles. We acknowledge the World Climate Research Programme's Working Group on Coupled Modelling, which is responsible for CMIP. We would like to express our gratitude to all the palynologists and geologists who, either directly or indirectly by providing their work to the Neotoma Paleoecology Database, contributed pollen data and chronologies to the dataset. The work of data contributors, data stewards, and the Neotoma community is gratefully acknowledged.

Data and code for reproducing results and figures of the manuscript are available on zenodo (Weitzel et al., 2022, `https://doi.org/10.5281/zenodo.6376036`). The modern calibration data, fossil pollen data, and code for computing the WAPLS reconstructions is available at Herzschuh et al. (2022a,b). The fossil data is part of a global pollen compilation with harmonized chronologies and taxonomy available at Herzschuh et al. (2022c, 2021).

Conflict of interest

The authors declare that they have no conflict of interest.

7 References

Abe-Ouchi, A., Saito, F., Kageyama, M., Braconnot, P., Harrison, S. P., Lambeck, K., Otto-Bliesner, B. L., Peltier, W. R., Tarasov, L., Peterschmitt, J. Y., and Takahashi, K.: Ice-sheet configuration in the CMIP5/PMIP3 Last Glacial Maximum experiments, Geoscientific Model Development, 8, 3621–3637, https://doi.org/10.5194/gmd-8-3621-2015, 2015.

Adam, M., Weitzel, N., and Rehfeld, K.: Identifying GlobalScale Patterns of Vegetation Change During the Last Deglaciation From Paleoclimate Networks, Paleoceanography and Paleoclimatology, 36, https://doi.org/10.1029/2021PA004265, 2021.

Alfimov, A. V. and Berman, D. I.: Beringian climate during the Late Pleistocene and Holocene, Quaternary Science Reviews, 20, 127–134, https://doi.org/10.1016/S0277-3791(00)00128-1, 2001.

Amante, C. and Eakins, B. W.: ETOPO1 1 Arc-Minute Global Relief Model: Procedures, Data Sources and Analysis, Tech. rep., URL `https://www.ngdc.noaa.gov/mgg/global/relief/ETOPO1/docs/ETOPO1.pdf`, 2009.

Anderson, P. and Lozhkin, A., eds.: Late Quaternary Vegetation and Climate of Siberia and the Russian Far East (Palynological and Radiocarbon Database), North East Science Center, Far East Branch, Russian Academy of Sciences, Magadan, Russia, 2002.

Anderson, P. M. and Lozhkin, A. V.: Late Quaternary vegetation of Chukotka (Northeast Russia), implications for Glacial and Holocene environments of Beringia, Quaternary Science Reviews, 107, 112–128, https://doi.org/10.1016/j.quascirev.2014.10.016, 2015.

Anderson, P. M., Belaya, B. V., Glushkova, O., and Lozhkin, A. V.: New data about the vegetation history of northern Priokhot'ye during the Late Pleistocene and Holocene (in Russian), in: Late Pleistocene and Holocene of Beringia, edited by Gagiev, M. K., pp. 33–54, North East Interdisciplinary Research Institute, Far East Branch, Russian Academy of Sciences, Magadan, Russia, 1997.

Anderson, P. M., Lozhkin, A. V., and Belaya, B. V.: Younger Dryas in western Beringia (northeastern Siberia) (in Russian), in: Environmental changes in Beringia during the Quaternary, edited by

Simakov, K. V., pp. 28–44, North East Interdisciplinary Research Institute, Far East Branch, Russian Academy of Sciences, Magadan, Russia, 1998a.

Anderson, P. M., Lozhkin, A. V., Belaya, B. V., and Stetsenko, T. V.: New data about the stratigraphy of late Quaternary deposits of northern Priokhot'ye (in Russian), in: Environmental changes in Beringia during the Quaternary, edited by Simakov, K. V., pp. 69–87, North East Interdisciplinary Research Institute, Far East Branch, Russian Academy of Sciences, Magadan, Russia, 1998b.

Anderson, P. M., Lozhkin, A. V., Solomatkina, T. B., and Brown, T. A.: Paleoclimatic implications of glacial and postglacial refugia for Pinus pumila in western Beringia, Quaternary Research, 73, 269–276, https://doi.org/10.1016/j.yqres.2009.09.008, 2010.

Andreev, A. A., Schirrmeister, L., Siegert, C., Bobrov, A. A., Demske, D., Seiffert, M., and Hubberten, H. W.: Paleoenvironmental changes in Northeastern Siberia during the Late Quaternary -Evidence from pollen records of the Bykovsky Peninsula, Polarforschung, 70, 13–25, 2000.

Andreev, A. A., Siegert, C., Klimanov, V. A., Derevyagin, A. Y., Shilova, G. N., and Melles, M.: Late Pleistocene and Holocene vegetation and climate on the Taymyr Lowland, Northern Siberia, Quaternary Research, 57, 138–150, https://doi.org/10.1006/qres.2001.2302, 2002.

Andreev, A. A., Tarasov, P. E., Siegert, C., Ebel, T., Klimanov, V. A., Melles, M., Bobrov, A. A., Dereviagin, A. Y., Lubinski, D. J., and Hubberten, H. W.: Late Pleistocene and Holocene vegetation and climate on the northern Taymyr Peninsula, Arctic Russia, Boreas, 32, 484–505, https://doi.org/10.1080/03009480310003388, 2003.

Andreev, A. A., Tarasov, P. E., Klimanov, V. A., Melles, M., Lisitsyna, O. M., and Hubberten, H. W.: Vegetation and climate changes around the Lama Lake, Taymyr Peninsula, Russia during the Late Pleistocene and Holocene, Quaternary International, 122, 69–84, https://doi.org/10.1016/j.quaint.2004.01.032, 2004.

Andreev, A. A., Schirrmeister, L., Tarasov, P. E., Ganopolski, A., Brovkin, V., Siegert, C., Wetterich, S., and Hubberten, H. W.: Vegetation and climate history in the Laptev Sea region (Arctic Siberia) during Late Quaternary inferred from pollen records, Quaternary Science Reviews, 30, 2182–2199, https://doi.org/10.1016/j.quascirev.2010.12.026, 2011.

Annan, J. D. and Hargreaves, J. C.: A new global reconstruction of temperature changes at the Last Glacial Maximum, Climate of the Past, 9, 367–376, https://doi.org/10.5194/cp-9-367-2013, 2013.

Ashastina, K., Kuzmina, S., Rudaya, N., Troeva, E., Schoch, W. H., Römermann, C., Reinecke, J., Otte, V., Savvinov, G., Wesche, K., and Kienast, F.: Woodlands and steppes: Pleistocene vegetation in Yakutia's most continental part recorded in the Batagay permafrost sequence, Quaternary Science Reviews, 196, 38–61, https://doi.org/10.1016/j.quascirev.2018.07.032, 2018.

Bakker, P., Rogozhina, I., Merkel, U., and Prange, M.: Hypersensitivity of glacial summer temperatures in Siberia, Climate of the Past, 16, 371–386, https://doi.org/10.5194/cp-16-371-2020, 2020.

Bartlein, P. J., Harrison, S. P., Brewer, S., Connor, S., Davis, B. A. S., Gajewski, K., Guiot, J., Harrison-Prentice, T. I., Henderson, A., Peyron, O., Prentice, I. C., Scholze, M., Seppä, H., Shuman, B., Sugita, S., Thompson, R. S., Viau, A. E., Williams, J., and Wu, H.: Pollen-based continental climate reconstructions at 6 and 21 ka: a global synthesis, Climate Dynamics, 37, 775–802, https://doi.org/10.1007/s00382-010-0904-1, 2011.

Batchelor, C. L., Margold, M., Krapp, M., Murton, D. K., Dalton, A. S., Gibbard, P. L., Stokes, C. R., Murton, J. B., and Manica, A.: The configuration of Northern Hemisphere ice sheets through the Quaternary, Nature Communications, 10, 1–10, https://doi.org/10.1038/s41467-019-11601-2, 2019.

Baumer, M. M., Wagner, B., Meyer, H., Leicher, N., Lenz, M., Fedorov, G., Pestryakova, L. A., and Melles, M.: Climatic and environmental changes in the Yana Highlands of northeastern Siberia over the last c . 57 000 years, derived from a sediment core from Lake Emanda, Boreas, 50, 114–133, https://doi.org/10.1111/bor.12476, 2021.

Berman, D., Alfimov, A., and Kuzmina, S.: Invertebrates of the relict steppe ecosystems of Beringia, and the reconstruction of Pleistocene landscapes, Quaternary Science Reviews, 30, 2200–2219, https://doi.org/10.1016/j.quascirev.2010.09.016, 2011.

Bezrukova, E. V., Tarasov, P. E., Solovieva, N., Krivonogov, S. K., and Riedel, F.: Last glacial-interglacial vegetation and environmental dynamics in southern Siberia: Chronology, forcing and feedbacks, Palaeogeography, Palaeoclimatology, Palaeoecology, 296, 185–198, https://doi.org/10.1016/j.palaeo.2010.07.020, 2010.

Birks, H. J. B., Heiri, O., Seppä, H., and Bjune, A. E.: Strengths and Weaknesses of Quantitative Climate Reconstructions Based on Late-Quaternary Biological Proxies, The Open Ecology Journal, 3, 68–110, https://doi.org/10.2174/1874213001003020068, 2010.

Blaauw, M. and Christen, J. A.: Flexible Paleoclimate Age-Depth Models Using an Autoregressive Gamma Process, Bayesian Analysis, 6, 457–474, https://doi.org/10.1214/11-BA618, 2011.

Braconnot, P., Harrison, S. P., Otto-Bliesner, B., Abe-Ouchi, A., Jungclaus, J., and Peterschmitt, J.-Y.: The Paleoclimate Modeling Intercomparison Project contribution to CMIP5, CLIVAR Exchanges, 56/16/2, 15–19, 2011.

Braconnot, P., Harrison, S. P., Kageyama, M., Bartlein, P. J., Masson-Delmotte, V., Abe-Ouchi, A., Otto-Bliesner, B., and Zhao, Y.: Evaluation of climate models using palaeoclimatic data, Nature Climate Change, 2, 417–424, https://doi.org/10.1038/NCLIMATE1456, 2012.

Budich, R., Giorgetta, M., Jungclaus, J. H., and Reick, C. H.: The MPI-M Millennium Earth System Model : An Assembling Guide for the COSMOS Configuration, Tech. rep., 2010.

Cao, X., Herzschuh, U., Telford, R., and Ni, J.: A modern pollen-climate dataset from China and Mongolia: Assessing its potential for climate reconstructions, Review of Palaeobotany and Palynology, 211, 87–96, https://doi.org/10.1016/j.revpalbo.2014.08.007, 2014.

Cao, X., Tian, F., Andreev, A., Anderson, P. M., Lozhkin, A. V., Bezrukova, E., Ni, J., Rudaya, N., Stobbe, A., Wieczorek, M., and Herzschuh, U.: A taxonomically harmonized and temporally standardized fossil pollen dataset from Siberia covering the last 40 kyr, Earth System Science Data, 12, 119–135, https://doi.org/10.5194/essd-12-119-2020, 2020.

Chevalier, M., Davis, B. A., Heiri, O., Seppä, H., Chase, B. M., Gajewski, K., Lacourse, T., Telford, R. J., Finsinger, W., Guiot, J., Kühl, N., Maezumi, S. Y., Tipton, J. R., Carter, V. A., Brussel, T., Phelps, L. N., Dawson, A., Zanon, M., Vall, F., Nolan, C., Mauri, A., de Vernal, A., Izumi, K., Holmström, L., Marsicek, J., Goring, S., Sommer, P. S., Chaput, M., and Kupriyanov, D.: Pollen-based climate reconstruction techniques for late Quaternary studies, Earth-Science Reviews, 210, 103 384, https://doi.org/10.1016/j.earscirev.2020.103384, 2020.

Cleator, S. F., Harrison, S. P., Nichols, N. K., Prentice, I. C., and Roulstone, I.: A new multivariable benchmark for Last Glacial Maximum climate simulations, Climate of the Past, 16, 699–712, https://doi.org/10.5194/cp-16-699-2020, 2020.

Colman, S. M., Peck, J. A., Karabanov, E. B., Carter, S. J., Bradbury, J. P., King, J. W., and Williams, D. F.: Continental climate response to orbital forcing from biogenic silica records in lake baikal, Nature, 378, 769–771, https://doi.org/10.1038/378769a0, 1995.

Cowling, S. A. and Sykes, M. T.: Physiological Significance of Low Atmospheric CO2 for PlantClimate Interactions, Quaternary Research, 52, 237–242, https://doi.org/https://doi.org/10.1006/qres.1999.2065, 1999.

Cramer, W., Bondeau, A., Woodward, F. I., Prentice, I. C., Betts, R. A., Brovkin, V., Cox, P. M., Fisher, V., Foley, J. A., Friend, A. D., Kucharik, C., Lomas, M. R., Ramankutty, N., Sitch, S., Smith, B., White, A., and Young-Molling, C.: Global response of terrestrial ecosystem structure and function to CO $_2$ and climate change: results from six dynamic global vegetation models:, Global Change Biology, 7, 357–373, https://doi.org/10.1046/j.1365-2486.2001.00383.x, 2001.

Demske, D., Heumann, G., Granoszewski, W., Nita, M., Mamakowa, K., Tarasov, P. E., and Oberhänsli, H.: Late glacial and Holocene vegetation and regional climate variability evidenced in high-resolution pollen records from Lake Baikal, Global and Planetary Change, 46, 255–279, https://doi.org/10.1016/j.gloplacha.2004.09.020, 2005.

Dorofeeva, R. P., Shen, P. Y., and Shapova, M. V.: Ground surface temperature histories inferred from deep borehole temperature-depth data in Eastern Siberia, Earth and Planetary Science Letters, 203, 1059–1071, https://doi.org/10.1016/S0012-821X(02)00925-1, 2002.

Dufresne, J. L., Foujols, M. A., Denvil, S., Caubel, A., Marti, O., Aumont, O., Balkanski, Y., Bekki, S., Bellenger, H., Benshila, R., Bony, S., Bopp, L., Braconnot, P., Brockmann, P., Cadule, P., Cheruy, F., Codron, F., Cozic, A., Cugnet, D., de Noblet, N., Duvel, J. P., Ethé, C., Fairhead, L., Fichefet, T., Flavoni, S., Friedlingstein, P., Grandpeix, J. Y., Guez, L., Guilyardi, E., Hauglustaine, D., Hourdin, F., Idelkadi, A., Ghattas, J., Joussaume, S., Kageyama, M., Krinner, G., Labetoulle, S., Lahellec, A., Lefebvre, M. P., Lefevre, F., Levy, C., Li, Z. X., Lloyd, J., Lott, F., Madec, G., Mancip, M., Marchand, M., Masson, S., Meurdesoif, Y., Mignot, J., Musat, I., Parouty, S., Polcher, J., Rio, C., Schulz, M., Swingedouw, D., Szopa, S., Talandier, C., Terray, P., Viovy, N., and Vuichard, N.: Climate change projections using the IPSL-CM5 Earth System Model: From CMIP3 to CMIP5, Climate Dynamics, 40, 2123–2165, https://doi.org/10.1007/s00382-012-1636-1, 2013.

Fick, S. E. and Hijmans, R. J.: WorldClim 2: new 1km spatial resolution climate surfaces for global land areas, International Journal of Climatology, 37, 4302–4315, https://doi.org/10.1002/joc.5086, 2017.

Gent, P. R., Danabasoglu, G., Donner, L. J., Holland, M. M., Hunke, E. C., Jayne, S. R., Lawrence, D. M., Neale, R. B., Rasch, P. J., Vertenstein, M., Worley, P. H., Yang, Z. L., and Zhang, M.: The community climate system model version 4, Journal of Climate, 24, 4973–4991, https://doi.org/10.1175/2011JCLI4083.1, 2011.

Giorgetta, M. A., Jungclaus, J., Reick, C. H., Legutke, S., Bader, J., Böttinger, M., Brovkin, V., Crueger, T., Esch, M., Fieg, K., Glushak, K., Gayler, V., Haak, H., Hollweg, H.-D., Ilyina, T., Kinne, S., Kornblueh, L., Matei, D., Mauritsen, T., Mikolajewicz, U., Mueller, W., Notz, D., Pithan, F., Raddatz, T., Rast, S., Redler, R., Roeckner, E., Schmidt, H., Schnur, R., Segschneider, J., Six, K. D., Stockhause, M., Timmreck, C., Wegner, J., Widmann, H., Wieners, K.-H., Claussen, M., Marotzke, J., and Stevens, B.: Climate and carbon cycle changes from 1850 to 2100 in MPI-ESM simulations for the Coupled Model Intercomparison Project phase 5, Journal of Advances in Modeling Earth Systems, 5, 572–597, https://doi.org/10.1002/jame.20038, 2013.

Guiot, J., Torre, F., Jolly, D., Peyron, O., Boreux, J., and Cheddadi, R.: Inverse vegetation modeling by Monte Carlo sampling to reconstruct palaeoclimates under changed precipitation seasonality and CO2 conditions: application to glacial climate in Mediterranean region, Ecological Modelling, 127, 119–140, https://doi.org/10.1016/S0304-3800(99)00219-7, 2000.

Hajima, T., Watanabe, M., Yamamoto, A., Tatebe, H., Noguchi, M. A., Abe, M., Ohgaito, R., Ito, A., Yamazaki, D., Okajima, H., Ito, A., Takata, K., Ogochi, K., Watanabe, S., and Kawamiya, M.: Development of the MIROC-ES2L Earth system model and the evaluation of biogeochemical processes and feedbacks, Geoscientific Model Development, 13, 2197–2244, https://doi.org/10.5194/gmd-13-2197-2020, 2020.

Hargreaves, G. H.: Defining and Using Reference Evapotranspiration, Journal of Irrigation and Drainage Engineering, 120, 1132–1139, https://doi.org/10.1061/(ASCE)0733-9437(1994)120:6(1132), 1994.

Harris, I., Osborn, T. J., Jones, P., and Lister, D.: Version 4 of the CRU TS monthly high-resolution gridded multivariate climate dataset, Scientific Data, 7, 109, https://doi.org/10.1038/s41597-020-0453-3, 2020.

Harrison, S. P. and Prentice, C. I.: Climate and CO $_2$ controls on global vegetation distribution at the last glacial maximum: analysis based on palaeovegetation data, biome modelling and palaeoclimate simulations, Global Change Biology, 9, 983–1004, https://doi.org/10.1046/j.1365-2486.2003.00640.x, 2003.

Herzschuh, U., Böhmer, T., Li, C., Cao, X., Heim, B., and Wieczorek, M.: Global taxonomically harmonized pollen data set for Late Quaternary with revised chronologies (LegacyPollen 1.0), https://doi.org/10.1594/PANGAEA.929773, 2021.

Herzschuh, U., Böhmer, T., Li, C., Chevalier, M., Dallmeyer, A., Cao, X., Bigelow, N. H., Nazarova, L., Novenko, E. Y., Park, J., Peyron, O., Rudaya, N. A., Schlütz, F., Shumilovskikh, L. S., Tarasov, P. E., Wang, Y., Wen, R., Xu, Q., and Zheng, Z.: LegacyClimate 1.0: A dataset of pollen-based climate reconstructions from 2594 Northern Hemisphere sites covering the late Quaternary, Earth System Science Data Discussions, 2022, 1–29, https://doi.org/10.5194/essd-2022-38, 2022a.

Herzschuh, U., Böhmer, T., Li, C., Chevalier, M., Dallmeyer, A., Cao, X., Bigelow, N. H., Nazarova, L., Novenko, E. Y., Park, J., Peyron, O., Rudaya, N. A., Schlütz, F., Shumilovskikh, L. S., Tarasov, P. E., Wang, Y., Wen, R., Xu, Q., and Zheng, Z.: LegacyClimate 1.0: A dataset of pollen-based climate reconstructions from 2594 Northern Hemisphere sites covering the late Quaternary, https://doi.org/10.5281/zenodo.5910989, 2022b.

Herzschuh, U., Li, C., Böhmer, T., Postl, A. K., Heim, B., Andreev, A. A., Cao, X., Wieczorek, M., and Ni, J.: LegacyPollen 1.0: A taxonomically harmonized global Late Quaternary pollen dataset of 2831 records with standardized chronologies, Earth System Science Data Discussions, 2022, 1–25, https://doi.org/10.5194/essd-2022-37, 2022c.

Hill, M. O.: Diversity and Evenness: A Unifying Notation and Its Consequences, Ecology, 54, 427–432, 1973.

Hughes, A. L. C., Gyllencreutz, R., Lohne, O. S., Mangerud, J., and Svendsen, J. I.: The last Eurasian ice sheets - a chronological database and time-slice reconstruction, DATED-1, Boreas, 45, 1–45, https://doi.org/10.1111/bor.12142, 2015.

Hughes, P. D., Gibbard, P. L., and Ehlers, J.: Timing of glaciation during the last glacial cycle: Evaluating the concept of a global 'Last Glacial Maximum' (LGM), Earth-Science Reviews, 125, 171–198, https://doi.org/10.1016/j.earscirev.2013.07.003, 2013.

Ivanov, V. F.: Quaternary deposits of the coast of eastern Chukotka (in Russian), Far Eastern Branch, USSR Academy of Sciences, Vladivostok, 1986.

Izumi, K. and Bartlein, P. J.: North American paleoclimate reconstructions for the Last Glacial Maximum using an inverse modeling through iterative forward modeling approach applied to pollen data: Pollen-Based Climate Reconstruction, Geophysical Research Letters, 43, 10,965–10,972, https://doi.org/10.1002/2016GL070152, 2016.

Jeltsch-Thömmes, A., Battaglia, G., Cartapanis, O., Jaccard, S. L., and Joos, F.: Low terrestrial carbon storage at the Last Glacial Maximum: Constraints from multi-proxy data, Climate of the Past, 15, 849–879, https://doi.org/10.5194/cp-15-849-2019, 2019.

Juggins, S.: Quantitative reconstructions in palaeolimnology: new paradigm or sick science?, Quaternary Science Reviews, 64, 20–32, https://doi.org/10.1016/j.quascirev.2012.12.014, 2013.

Juggins, S.: rioja: Analysis of Quaternary Science Data, URL https://cran.r-project.org/package=rioja, r package version 0.9-26, 2020.

Juggins, S. and Birks, H. J. B.: Quantitative Environmental Reconstructions from Biological Data, in: Tracking Environmental Change Using Lake Sediments: Data Handling and Numerical Techniques, edited by Birks, H. J. B., Lotter, A. F., Juggins, S., and Smol, J. P., pp. 431–494, Springer Netherlands, Dordrecht, 2012.

Kageyama, M., Albani, S., Braconnot, P., Harrison, S. P., Hopcroft, P. O., Ivanovic, R. F., Lambert, F., Marti, O., Peltier, W. R., Peterschmitt, J.-Y., Roche, D. M., Tarasov, L., Zhang, X., Brady, E. C., Haywood, A. M., LeGrande, A. N., Lunt, D. J., Mahowald, N. M., Mikolajewicz, U., Nisancioglu, K. H., Otto-Bliesner, B. L., Renssen, H., Tomas, R. A., Zhang, Q., Abe-Ouchi, A., Bartlein, P. J., Cao, J., Li, Q., Lohmann, G., Ohgaito, R., Shi, X., Volodin, E., Yoshida, K., Zhang, X., and Zheng, W.: The PMIP4 contribution to CMIP6 – Part 4: Scientific objectives and experimental design of the PMIP4-CMIP6 Last Glacial Maximum experiments and PMIP4 sensitivity experiments, Geoscientific Model Development, 10, 4035–4055, https://doi.org/10.5194/gmd-10-4035-2017, 2017.

Kageyama, M., Harrison, S. P., Kapsch, M.-L., Lofverstrom, M., Lora, J. M., Mikolajewicz, U., Sherriff-Tadano, S., Vadsaria, T., Abe-Ouchi, A., Bouttes, N., Chandan, D., Gregoire, L. J., Ivanovic, R. F., Izumi, K., LeGrande, A. N., Lhardy, F., Lohmann, G., Morozova, P. A., Ohgaito, R., Paul, A., Peltier, W. R., Poulsen, C. J., Quiquet, A., Roche, D. M., Shi, X., Tierney, J. E., Valdes, P. J., Volodin, E., and Zhu, J.: The PMIP4 Last Glacial Maximum experiments: preliminary results and comparison with the PMIP3 simulations, Climate of the Past, 17, 1065–1089, https://doi.org/10.5194/cp-17-1065-2021, 2021.

Kiefer, T., Sarnthein, M., Erlenkeuser, H., Grootes, P. M., and Roberts, A. P.: North Pacific response to millennial-scale changes in ocean circulation over the last 60 kyr, Paleoceanography, 16, 179–189, https://doi.org/10.1029/2000PA000545, 2001.

Kienast, F., Schirrmeister, L., Siegert, C., and Tarasov, P.: Palaeobotanical evidence for warm summers in the East Siberian Arctic during the last cold stage, Quaternary Research, 63, 283–300, https://doi.org/10.1016/j.yqres.2005.01.003, 2005.

Köhler, P., Nehrbass-Ahles, C., Schmitt, J., Stocker, T. F., and Fischer, H.: A 156 kyr smoothed history of the atmospheric greenhouse gases CO2, CH4, and N2O and their radiative forcing, Earth System Science Data, 9, 363–387, https://doi.org/10.5194/essd-9-363-2017, 2017.

Krinner, G., Boucher, O., and Balkanski, Y.: Ice-free glacial northern Asia due to dust deposition on snow, Climate Dynamics, 27, 613–625, https://doi.org/10.1007/s00382-006-0159-z, 2006.

Lambeck, K., Rouby, H., Purcell, A., Sun, Y., and Sambridge, M.: Sea level and global ice volumes from the Last Glacial Maximum to the Holocene, Proceedings of the National Academy of Sciences, 111, 15 296–15 303, https://doi.org/10.1073/pnas.1411762111, 2014.

Leipe, C., Nakagawa, T., Gotanda, K., Müller, S., and Tarasov, P. E.: Late Quaternary vegetation and climate dynamics at the northern limit of the East Asian summer monsoon and its regional and global-scale controls, Quaternary Science Reviews, 116, 57–71, https://doi.org/10.1016/j.quascirev.2015.03.012, 2015.

Li, C., Postl, A. K., Böhmer, T., Cao, X., Dolman, A. M., and Herzschuh, U.: Harmonized chronologies of a global late Quaternary pollen dataset (LegacyAge 1.0), Earth System Science Data Discussions, 2021, 1–24, https://doi.org/10.5194/essd-2021-212, 2021.

Li, L., Lin, P., Yu, Y., Wang, B., Zhou, T., Liu, L., Liu, J., Bao, Q., Xu, S., Huang, W., Xia, K., Pu, Y., Dong, L., Shen, S., Liu, Y., Hu, N., Liu, M., Sun, W., Shi, X., Zheng, W., Wu, B., Song, M., Liu, H., Zhang, X., Wu, G., Xue, W., Huang, X., Yang, G., Song, Z., and Qiao, F.: The flexible global

ocean-atmosphere-land system model, Grid-point Version 2: FGOALS-g2, Advances in Atmospheric Sciences, 30, 543–560, https://doi.org/10.1007/s00376-012-2140-6, 2013.

Lindgren, A., Hugelius, G., and Kuhry, P.: Extensive loss of past permafrost carbon but a net accumulation into present-day soils, Nature, 560, 219–222, https://doi.org/10.1038/s41586-018-0371-0, 2018.

Lindgren, F., Rue, H., and Lindström, J.: An explicit link between Gaussian fields and Gaussian Markov random fields: the stochastic partial differential equation approach, Journal of the Royal Statistical Society, Statistical Methodology, Series B, 73, 423–498, https://doi.org/10.1111/j.1467-9868.2011.00777.x, 2011.

Löfverström, M., Caballero, R., Nilsson, J., and Kleman, J.: Evolution of the large-scale atmospheric circulation in response to changing ice sheets over the last glacial cycle, Climate of the Past, 10, 1453–1471, https://doi.org/10.5194/cp-10-1453-2014, 2014.

Lozhkin, A. and Anderson, P.: Late Quaternary lake records from the Anadyr Lowland, Central Chukotka (Russia), Quaternary Science Reviews, 68, 1–16, https://doi.org/10.1016/j.quascirev.2013.02.007, 2013.

Lozhkin, A. V.: Questions concerning radiocarbon data and palynological characteristics of the mammoth burials, Berelyekh River, lower Indigirka drainage (in Russian), in: Environmental changes in Beringia during the Quaternary, edited by Simakov, K. V., pp. 45–62, North East Interdisciplinary Research Institute, Far East Branch, Russian Academy of Sciences, Magadan, Russia, 1998.

Lozhkin, A. V. and Glushkova, O. Y.: Boreal peats in the upper Kolyma basin (in Russian), in: Late Pleistocene and Holocene of Beringia, edited by Gagiev, M. K., pp. 55–62, North East Interdisciplinary Research Institute, Far East Branch, Russian Academy of Sciences, Magadan, Russia, 1997.

Lozhkin, A. V. and Postolenko, G. A.: New data about the environmental evolution of the mountain region of the Kolyma region during the late Anthropogene (in Russian), Doklady Akademii Nauk, 307, 1184–1188, 1989.

Lozhkin, A. V., Pavlov, G. F., Ryabchun, V. K., Gorbachev, A. L., Zadal'skii, S. V., and Schubert, E. E.: A new mammoth discovery in Chukotka (in Russian), Doklady Akademii Nauk, 302, 1440–1444, 1988.

Lozhkin, A. V., Anderson, P. M., Eisner, W. R., Ravako, L. G., Hopkins, D. M., Brubaker, L. B., Colinvaux, P. A., and Miller, M. C.: Late quaternary lacustrine pollen records from southwestern beringia, Quaternary Research, 39, 314–324, https://doi.org/10.1006/qres.1993.1038, 1993.

Lozhkin, A. V., Anderson, P. M., and Belaya, B. V.: Radiocarbon dates and carbon zones from lacustrine sediments from the region of the Kolyma-Okhotsk drainage divide (in Russian), Doklady Akademii Nauk, 343, 396–399, 1995.

Lozhkin, A. V., Anderson, P. M., Brubaker, L. B., Kotov, A. N., Kotova, L. N., and Prokhorova, T. P.: The herb pollen zone from sediments of glacial lakes (in Russian), in: Environmental changes in Beringia during the Quaternary, edited by Simakov, K. V., pp. 96–111, North East Interdisciplinary Research Institute, Far East Branch, Russian Academy of Sciences, Magadan, Russia, 1998a.

Lozhkin, A. V., Hopkins, D. M., Solomatkina, T. B., Eisner, W. R., and Brigham-Grette, J.: Radiocarbon dates and palynological characteristics of peat from St Lawrence Island (in Russian), in: Environmental changes in Beringia during the Quaternary, edited by Simakov, K. V., pp. 9–27, North East Interdisciplinary Research Institute, Far East Branch, Russian Academy of Sciences, Magadan, Russia, 1998b.

Lozhkin, A. V., Kotov, A. N., and Ryabchun, V. K.: Palynological and radiocarbon data of the Ledovyi Obryv exposure (the south east of Chukotka) (in Russian), in: The Quaternary Period of Beringia,

edited by Simakov, K. V., pp. 118–131, North East Interdisciplinary Research Institute, Far East Branch, Russian Academy of Sciences, Magadan, Russia, 2000.

Lozhkin, A. V., Anderson, P. M., Matrosova, T. V., and Minyuk, P. S.: The pollen record from El'gygytgyn Lake: Implications for vegetation and climate histories of northern Chukotka since the late middle Pleistocene, Journal of Paleolimnology, 37, 135–153, https://doi.org/10.1007/s10933-006-9018-5, 2007.

Lozhkin A. V. and Anderson, P. M.: A late Quaternary pollen record from Elikchan 4 Lake, northeast Siberia, Geology of the Pacific Ocean, 14, 18–22, 1995.

Ma, Y., Liu, K.-b., Feng, Z., Meng, H., Sang, Y., Wang, W., and Zhang, H.: Vegetation changes and associated climate variations during the past 38,000 years reconstructed from the Shaamar eolian-paleosol section, northern Mongolia, Quaternary International, 311, 25–35, https://doi.org/10.1016/j.quaint.2013.08.037, 2013.

MARGO Project Members: Constraints on the magnitude and patterns of ocean cooling at the Last Glacial Maximum, Nature Geoscience, 2, 127–132, https://doi.org/10.1038/ngeo411, 2009.

Mauritsen, T., Bader, J., Becker, T., Behrens, J., Bittner, M., Brokopf, R., Brovkin, V., Claussen, M., Crueger, T., Esch, M., Fast, I., Fiedler, S., Fläschner, D., Gayler, V., Giorgetta, M., Goll, D. S., Haak, H., Hagemann, S., Hedemann, C., Hohenegger, C., Ilyina, T., Jahns, T., JimenzdelaCuesta, D., Jungclaus, J., Kleinen, T., Kloster, S., Kracher, D., Kinne, S., Kleberg, D., Lasslop, G., Kornblueh, L., Marotzke, J., Matei, D., Meraner, K., Mikolajewicz, U., Modali, K., Möbis, B., Müller, W. A., Nabel, J. E. M. S., Nam, C. C. W., Notz, D., Nyawira, S., Paulsen, H., Peters, K., Pincus, R., Pohlmann, H., Pongratz, J., Popp, M., Raddatz, T. J., Rast, S., Redler, R., Reick, C. H., Rohrschneider, T., Schemann, V., Schmidt, H., Schnur, R., Schulzweida, U., Six, K. D., Stein, L., Stemmler, I., Stevens, B., Storch, J., Tian, F., Voigt, A., Vrese, P., Wieners, K., Wilkenskjeld, S., Winkler, A., and Roeckner, E.: Developments in the MPIM Earth System Model version 1.2 (MPIESM1.2) and Its Response to Increasing CO $_2$, Journal of Advances in Modeling Earth Systems, 11, 998–1038, https://doi.org/10.1029/2018MS001400, 2019.

Melles, M., Brigham-Grette, J., Minyuk, P. S., Nowaczyk, N. R., Wennrich, V., DeConto, R. M., Anderson, P. M., Andreev, A. A., Coletti, A., Cook, T. L., Haltia-Hovi, E., Kukkonen, M., Lozhkin, A. V., Rosén, P., Tarasov, P., Vogel, H., and Wagner, B.: 2.8 Million years of arctic climate change from Lake El'gygytgyn, NE Russia, Science, 337, 315–320, https://doi.org/10.1126/science.1222135, 2012.

Meyer, H., Dereviagin, A., Siegert, C., Schirrmeister, L., and Hubberten, H. W.: Palaeoclimate reconstruction on Big Lyakhovsky Island, North Siberia - Hydrogen and oxygen isotopes in ice wedges, Permafrost and Periglacial Processes, 13, 91–105, https://doi.org/10.1002/ppp.416, 2002.

Meyer, V. and Barr, I.: Linking glacier extent and summer temperature in NE Russia - Implications for precipitation during the global Last Glacial Maximum, Palaeogeography, Palaeoclimatology, Palaeoecology, 470, 72–80, https://doi.org/10.1016/j.palaeo.2016.12.038, 2017.

Meyer, V. D., Max, L., Hefter, J., Tiedemann, R., and Mollenhauer, G.: Glacial-to-Holocene evolution of sea surface temperature and surface circulation in the subarctic northwest Pacific and the Western Bering Sea, Paleoceanography, 31, 916–927, https://doi.org/10.1002/2015PA002877, 2016.

Meyer, V. D., Hefter, J., Lohmann, G., Max, L., Tiedemann, R., and Mollenhauer, G.: Summer temperature evolution on the Kamchatka Peninsula, Russian Far East, during the past 20 000 years, Climate of the Past, 13, 359–377, https://doi.org/10.5194/cp-13-359-2017, 2017.

Mokhova, L., Tarasov, P., Bazarova, V., and Klimin, M.: Quantitative biome reconstruction using modern and late Quaternary pollen data from the southern part of the Russian Far East, Quaternary Science Reviews, 28, 2913–2926, https://doi.org/10.1016/j.quascirev.2009.07.018, 2009.

Müller, S., Tarasov, P. E., Andreev, A. A., Tütken, T., Gartz, S., and Diekmann, B.: Late Quaternary vegetation and environments in the Verkhoyansk Mountains region (NE Asia) reconstructed from a 50-kyr fossil pollen record from Lake Billyakh, Quaternary Science Reviews, 29, 2071–2086, https://doi.org/10.1016/j.quascirev.2010.04.024, 2010.

Niu, L., Lohmann, G., Hinck, S., Gowan, E. J., and Krebs-Kanzow, U.: The sensitivity of Northern Hemisphere ice sheets to atmospheric forcing during the last glacial cycle using PMIP3 models, Journal of Glaciology, 65, 645–661, https://doi.org/10.1017/jog.2019.42, 2019.

O'ishi, R. and Abe-Ouchi, A.: Influence of dynamic vegetation on climate change and terrestrial carbon storage in the Last Glacial Maximum, Climate of the Past, 9, 1571–1587, https://doi.org/10.5194/cp-9-1571-2013, 2013.

Opel, T., Murton, J. B., Wetterich, S., Meyer, H., Ashastina, K., Günther, F., Grotheer, H., Mollenhauer, G., Danilov, P. P., Boeskorov, V., Savvinov, G. N., and Schirrmeister, L.: Past climate and continentality inferred from ice wedges at Batagay megaslump in the Northern Hemisphere's most continental region, Yana Highlands, interior Yakutia, Climate of the Past, 15, 1443–1461, https://doi.org/10.5194/cp-15-1443-2019, 2019.

Otto-Bliesner, B. L., Brady, E. C., Clauzet, G., Tomas, R., Levis, S., and Kothavala, Z.: Last glacial maximum and Holocene climate in CCSM3, Journal of Climate, 19, 2526–2544, https://doi.org/10.1175/JCLI3748.1, 2006.

Pitul'Ko, V. V., Pavlova, E. Y., Kuz'Mina, S. A., Nikol'Skii, P. A., Basilyan, A. E., Tumskoi, V. E., and Anisimov, M. A.: Natural-climatic changes in the Yana-Indigirka lowland during the terminal Kargino time and habitat of late Paleolithic man in northern part of East Siberia, Doklady Earth Sciences, 417, 1256–1260, https://doi.org/10.1134/S1028334X07080284, 2007.

Prentice, I. C., Dong, N., Gleason, S. M., Maire, V., and Wright, I. J.: Balancing the costs of carbon gain and water transport: testing a new theoretical framework for plant functional ecology, Ecology Letters, 17, 82–91, https://doi.org/10.1111/ele.12211, 2014.

Prentice, I. C., Cleator, S. F., Huang, Y. H., Harrison, S. P., and Roulstone, I.: Reconstructing ice-age palaeoclimates: Quantifying low-CO2 effects on plants, Global and Planetary Change, 149, 166–176, https://doi.org/10.1016/j.gloplacha.2016.12.012, 2017.

Rehfeld, K., Trachsel, M., Telford, R. J., and Laepple, T.: Assessing performance and seasonal bias of pollen-based climate reconstructions in a perfect model world, Climate of the Past, 12, 2255–2270, https://doi.org/10.5194/cp-12-2255-2016, 2016.

Reimer, P. J., Austin, W. E. N., Bard, E., Bayliss, A., Blackwell, P. G., Bronk Ramsey, C., Butzin, M., Cheng, H., Edwards, R. L., Friedrich, M., Grootes, P. M., Guilderson, T. P., Hajdas, I., Heaton, T. J., Hogg, A. G., Hughen, K. A., Kromer, B., Manning, S. W., Muscheler, R., Palmer, J. G., Pearson, C., van der Plicht, J., Reimer, R. W., Richards, D. A., Scott, E. M., Southon, J. R., Turney, C. S. M., Wacker, L., Adolphi, F., Büntgen, U., Capano, M., Fahrni, S. M., Fogtmann-Schulz, A., Friedrich, R., Köhler, P., Kudsk, S., Miyake, F., Olsen, J., Reinig, F., Sakamoto, M., Sookdeo, A., and Talamo, S.: The IntCal20 Northern Hemisphere Radiocarbon Age Calibration Curve (055 cal kBP), Radiocarbon, 62, 725–757, https://doi.org/10.1017/RDC.2020.41, 2020.

Salonen, J. S., Korpela, M., Williams, J. W., and Luoto, M.: Machine-learning based reconstructions of primary and secondary climate variables from North American and European fossil pollen data, Scientific Reports, 9, 15 805, https://doi.org/10.1038/s41598-019-52293-4, 2019.

Schmidt, G. A., Kelley, M., Nazarenko, L., Ruedy, R., Russell, G. L., Aleinov, I., Bauer, M., Bauer, S. E., Bhat, M. K., Bleck, R., Canuto, V., Chen, Y.-h., Cheng, Y., Clune, T. L., Genio, A. D., Fainchtein, R. D., Faluvegi, G., Hansen, J. E., Healy, R. J., Kiang, N. Y., Koch, D., Lacis, A. A., Legrande, A. N., Lerner, J., Lo, K. K., Matthews, E. E., Menon, S., Miller, R. L., Oinas, V., and Oloso, A. O.: Journal

of Advances in Modeling Earth Systems contributions to the CMIP5 archive, Journal of Advances in Modeling Earth Systems, 6, 141–184, https://doi.org/10.1002/2013MS000265.Received, 2014.

Seki, O., Sakamoto, T., Sakai, S., Schouten, S., Hopmans, E. C., Damste, J. S., and Pancost, R. D.: Large changes in seasonal sea ice distribution and productivity in the Sea of Okhotsk during the deglaciations, Geochemistry, Geophysics, Geosystems, 10, 1–10, https://doi.org/10.1029/2009GC002613, 2009.

Sher, A. V., Kuzmina, S. A., Kuznetsova, T. V., and Sulerzhitsky, L. D.: New insights into the Weichselian environment and climate of the East Siberian Arctic, derived from fossil insects, plants, and mammals, Quaternary Science Reviews, 24, 533–569, https://doi.org/10.1016/j.quascirev.2004.09.007, 2005.

Shichi, K., Takahara, H., Krivonogov, S. K., Bezrukova, E. V., Kashiwaya, K., Takehara, A., and Nakamura, T.: Late Pleistocene and Holocene vegetation and climate records from Lake Kotokel, central Baikal region, Quaternary International, 205, 98–110, https://doi.org/10.1016/j.quaint.2009.02.005, 2009.

Shilo, N. A., Lozhkin, A. V., Titov, E. E., and Schumilov, Y. V.: Kirgirlakh mammoth: paleography aspect (in Russian), Nauka, Moscow, 1983.

Sidorenko, D., Rackow, T., Jung, T., Semmler, T., Barbi, D., Danilov, S., Dethloff, K., Dorn, W., Fieg, K., Goessling, H. F., Handorf, D., Harig, S., Hiller, W., Juricke, S., Losch, M., Schröter, J., Sein, D. V., and Wang, Q.: Towards multi-resolution global climate modeling with ECHAM6FESOM. Part I: model formulation and mean climate, Climate Dynamics, 44, 757–780, https://doi.org/10.1007/s00382-014-2290-6, 2015.

Stauch, G. and Gualtieri, L.: Late Quaternary glaciations in northeastern Russia, Journal of Quaternary Science, 23, 545–558, https://doi.org/10.1002/jqs.1211, 2008.

Sueyoshi, T., Ohgaito, R., Yamamoto, A., Chikamoto, M. O., Hajima, T., Okajima, H., Yoshimori, M., Abe, M., Oishi, R., Saito, F., Watanabe, S., Kawamiya, M., and Abe-Ouchi, A.: Set-up of the PMIP3 paleoclimate experiments conducted using an Earth system model, MIROC-ESM, Geoscientific Model Development, 6, 819–836, https://doi.org/10.5194/gmd-6-819-2013, 2013.

Svendsen, J. I., Alexanderson, H., Astakhov, V. I., Demidov, I., Dowdeswell, J. A., Funder, S., Gataullin, V., Henriksen, M., Hjort, C., Houmark-Nielsen, M., Hubberten, H. W., Ingólfsson, Ó., Jakobsson, M., Kjær, K. H., Larsen, E., Lokrantz, H., Lunkka, J. P., Lysså, A., Mangerud, J., Matiouchkov, A., Murray, A., Möller, P., Niessen, F., Nikolskaya, O., Polyak, L., Saarnisto, M., Siegert, C., Siegert, M. J., Spielhagen, R. F., and Stein, R.: Late Quaternary ice sheet history of northern Eurasia, Quaternary Science Reviews, 23, 1229–1271, https://doi.org/10.1016/j.quascirev.2003.12.008, 2004.

Tarasov, P. E., Peyron, O., Guiot, J., Brewer, S., Volkova, V. S., Bezusko, L. G., Dorofeyuk, N. I., Kvavadze, E. V., Osipova, I. M., and Panova, N. K.: Last Glacial Maximum climate of the former Soviet Union and Mongolia reconstructed from pollen and plant macrofossil data, Climate Dynamics, 15, 227–240, https://doi.org/10.1007/s003820050278, 1999.

Tarasov, P. E., Bezrukova, E. V., and Krivonogov, S. K.: Late glacial and holocene changes in vegetation cover and climate in southern Siberia derived from a 15 kyr long pollen record from Lake Kotokel, Climate of the Past, 5, 285–295, https://doi.org/10.5194/cp-5-285-2009, 2009.

Telford, R. J. and Birks, H. J.: A novel method for assessing the statistical significance of quantitative reconstructions inferred from biotic assemblages, Quaternary Science Reviews, 30, 1272–1278, https://doi.org/10.1016/j.quascirev.2011.03.002, 2011.

Ter Braak, C. J. and Juggins, S.: Weighted averaging partial least squares regression (WA-PLS): an improved method for reconstructing environmental variables from species assemblages, Hydrobiologia, 269-270, 485–502, https://doi.org/10.1007/BF00028046, 1993.

Ter Braak, C. J. F., Juggins, S., Birks, H. J. B., and van der Voet, H.: Weighted averaging partial least squares regression (WA-PLS): Definition and comparison with other methods for species-environment calibration, in: Multivariate Environmental Statistics, edited by Patil, G. P. and Rao, C. R., pp. 525–560, Elsevier Science, 1993.

Tierney, J. E., Zhu, J., King, J., Malevich, S. B., Hakim, G. J., and Poulsen, C. J.: Glacial cooling and climate sensitivity revisited, Nature, 584, 569–573, https://doi.org/10.1038/s41586-020-2617-x, 2020.

Tipton, J. R., Hooten, M. B., Nolan, C., Booth, R. K., and McLachlan, J.: Predicting paleoclimate from compositional data using multivariate Gaussian process inverse prediction, The Annals of Applied Statistics, 13, https://doi.org/10.1214/19-AOAS1281, 2019.

Trabucco, A., Zomer, R. J., Bossio, D. A., van Straaten, O., and Verchot, L. V.: Climate change mitigation through afforestation/reforestation: A global analysis of hydrologic impacts with four case studies, Agriculture, Ecosystems & Environment, 126, 81–97, https://doi.org/10.1016/j.agee.2008.01.015, 2008.

van der Voet, H.: Comparing the predictive accuracy of models using a simple randomization test, Chemometrics and Intelligent Laboratory Systems, 25, 313–323, https://doi.org/10.1016/0169-7439(94)85050-X, 1994.

Volodin, E. M., Mortikov, E. V., Kostrykin, S. V., Galin, V. Y., Lykossov, V. N., Gritsun, A. S., Diansky, N. A., Gusev, A. V., Iakovlev, N. G., Shestakova, A. A., and Emelina, S. V.: Simulation of the modern climate using the INM-CM48 climate model, Russian Journal of Numerical Analysis and Mathematical Modelling, 33, 367–374, https://doi.org/doi:10.1515/rnam-2018-0032, 2018.

Vyse, S. A., Herzschuh, U., Andreev, A. A., Pestryakova, L. A., Diekmann, B., Armitage, S. J., and Biskaborn, B. K.: Geochemical and sedimentological responses of arctic glacial Lake Ilirney, chukotka (far east Russia) to palaeoenvironmental change since 51.8 ka BP, Quaternary Science Reviews, 247, 106 607, https://doi.org/10.1016/j.quascirev.2020.106607, 2020.

Wang, H., Prentice, I. C., Keenan, T. F., Davis, T. W., Wright, I. J., Cornwell, W. K., Evans, B. J., and Peng, C.: Towards a universal model for carbon dioxide uptake by plants, Nature Plants, 3, 734–741, https://doi.org/10.1038/s41477-017-0006-8, 2017.

Wei, D., Gonzlez-Sampriz, P., Gil-Romera, G., Harrison, S. P., and Prentice, I. C.: Seasonal temperature and moisture changes in interior semiarid Spain from the last interglacial to the Late Holocene, Quaternary Research, 101, 143–155, https://doi.org/10.1017/qua.2020.108, 2021.

Weitzel, N., Hense, A., and Ohlwein, C.: Combining a pollen and macrofossil synthesis with climate simulations for spatial reconstructions of European climate using Bayesian filtering, Climate of the Past, 15, 1275–1301, https://doi.org/10.5194/cp-15-1275-2019, 2019.

Weitzel, N., Hense, A., Herzschuh, U., Böhmer, T., Cao, X., and Rehfeld, K.: Code and data in supplement to "A state estimate of Siberian summer temperature and moisture availability during the Last Glacial Maximum combining pollen records and climate simulations", https://doi.org/10.5281/zenodo.6376036, 2022.

Wetterich, S., Rudaya, N., Tumskoy, V., Andreev, A. A., Opel, T., Schirrmeister, L., and Meyer, H.: Last Glacial Maximum records in permafrost of the East Siberian Arctic, Quaternary Science Reviews, 30, 3139–3151, https://doi.org/10.1016/j.quascirev.2011.07.020, 2011.

Wetterich, S., Meyer, H., Fritz, M., Mollenhauer, G., Rethemeyer, J., Kizyakov, A., Schirrmeister, L., and Opel, T.: Northeast Siberian Permafrost IceWedge Stable Isotopes Depict Pronounced Last Glacial Maximum Winter Cooling, Geophysical Research Letters, 48, https://doi.org/10.1029/2020GL092087, 2021.

Whittle, P.: Stochastic processes in several dimensions, Bulletin of the International Statistical Institute, 40, 974–994, 1963.

Williams, J. W., Webb, T., Shurman, B. N., and Bartlein, P. J.: Do Low CO $_2$ Concentrations Affect Pollen-Based Reconstructions of LGM Climates? A Response to Physiological Significance of Low Atmospheric CO $_2$ for PlantClimate Interactions by Cowling and Sykes, Quaternary Research, 53, 402–404, https://doi.org/10.1006/qres.2000.2131, 2000.

Wu, H., Guiot, J., Brewer, S., and Guo, Z.: Climatic changes in Eurasia and Africa at the last glacial maximum and mid-Holocene: reconstruction from pollen data using inverse vegetation modelling, Climate Dynamics, 29, 211–229, https://doi.org/10.1007/s00382-007-0231-3, 2007a.

Wu, H., Guiot, J., Brewer, S., Guo, Z., and Peng, C.: Dominant factors controlling glacial and interglacial variations in the treeline elevation in tropical Africa, Proceedings of the National Academy of Sciences, 104, 9720–9724, https://doi.org/10.1073/pnas.0610109104, 2007b.

Wu, H., Li, Q., Yu, Y., Sun, A., Lin, Y., Jiang, W., and Luo, Y.: Quantitative climatic reconstruction of the Last Glacial Maximum in China, Science China Earth Sciences, 62, 1269–1278, https://doi.org/10.1007/s11430-018-9338-3, 2019.

Yukimoto, S., Adachi, Y., Hosaka, M., Sakami, T., Yoshimura, H., Hirabara, M., Tanaka, T. Y., Shindo, E., Tsujino, H., Deushi, M., Mizuta, R., Yabu, S., Obata, A., Nakano, H., Koshiro, T., Ose, T., and Kitoh, A.: A new global climate model of the Meteorological Research Institute: MRI-CGCM3: -Model description and basic performance-, Journal of the Meteorological Society of Japan, 90, 23–64, https://doi.org/10.2151/jmsj.2012-A02, 2012.

Zech, R., Huang, Y., Zech, M., Tarozo, R., and Zech, W.: High carbon sequestration in Siberian permafrost loess-paleosols during glacials, Climate of the Past, 7, 501–509, https://doi.org/10.5194/cp-7-501-2011, 2011.